



Seismoelectric couplings in a poroelastic material containing two immiscible fluid phases

Abderrahim Jardani, A Revil

► To cite this version:

Abderrahim Jardani, A Revil. Seismoelectric couplings in a poroelastic material containing two immiscible fluid phases. *Geophysical Journal International*, 2015, 202 (2), pp.850–870. 10.1093/gji/ggv176 . hal-01742269

HAL Id: hal-01742269

<https://normandie-univ.hal.science/hal-01742269>

Submitted on 27 Jan 2021

HAL is a multi-disciplinary open access archive for the deposit and dissemination of scientific research documents, whether they are published or not. The documents may come from teaching and research institutions in France or abroad, or from public or private research centers.

L'archive ouverte pluridisciplinaire **HAL**, est destinée au dépôt et à la diffusion de documents scientifiques de niveau recherche, publiés ou non, émanant des établissements d'enseignement et de recherche français ou étrangers, des laboratoires publics ou privés.

Seismoelectric couplings in a poroelastic material containing two immiscible fluid phases

A. Jardani¹ and A. Revil^{2,3}

¹ Université de Rouen, M2C, UMR 6143, CNRS, Morphodynamique Continentale et Côtière Mont Saint Aignan, France.

E-mail: abderrahim.jardani@univ-rouen.fr

² Colorado School of Mines, Department of Geophysics, Golden, CO, USA

³ ISTerre, CNRS, UMR 5275, Université de Savoie, Equipe Volcan, Le Bourget du Lac, France

Accepted 2015 April 21. Received 2015 April 21; in original form 2014 August 18

SUMMARY

A new approach of seismoelectric imaging has been recently proposed to detect saturation fronts in which seismic waves are focused in the subsurface to scan its heterogeneous nature and determine saturation fronts. Such type of imaging requires however a complete modelling of the seismoelectric properties of porous media saturated by two immiscible fluid phases, one being usually electrically insulating (for instance water and oil). We combine an extension of Biot dynamic theory, valid for porous media containing two immiscible Newtonian fluids, with an extension of the electrokinetic theory based on the notion of effective volumetric charge densities dragged by the flow of each fluid phase. These effective charge densities can be related directly to the permeability and saturation of each fluid phase. The coupled partial differential equations are solved with the finite element method. We also derive analytically the transfer function connecting the macroscopic electrical field to the acceleration of the fast *P* wave (coseismic electrical field) and we study the influence of the water content on this coupling. We observe that the amplitude of the co-seismic electrical disturbance is very sensitive to the water content with an increase in amplitude with water saturation. We also investigate the seismoelectric conversions (interface effect) occurring at the water table. We show that the conversion response at the water table can be identifiable only when the saturation contrasts between the vadose and saturated zones are sharp enough. A relatively dry vadose zone represents the best condition to identify the water table through seismoelectric measurements. Indeed, in this case, the coseismic electrical disturbances are vanishingly small compared to the seismoelectric interface response.

Key words: Geomechanics; Hydrogeophysics.

1 INTRODUCTION

The seismoelectric method consists in measuring the electric fields associated with the propagation of seismic waves in a porous medium partially or fully saturated by an aqueous fluid phase (Haartsen & Pride 1997; Garambois & Dietrich 2001; Pride & Garambois 2005; Haines & Pride 2006; Dupuis *et al.* 2009). This method has a long history in geophysics (e.g. Ivanov 1939; Frenkel 1944; Martner & Sparks 1959) but a rigorous theory of the seismoelectric effects has only been available since the seminal work of Pride (1994). The conversion of mechanical to electromagnetic energy is due to the existence of the electrical double layer at the pore water–solid interface and the resulting coupling is said to be electrokinetic in nature. Minerals in contact with water develop indeed an electrical charge on their surface because of amphoteric (pH-dependent) reactions on their surface. This surface charge is counterbalanced by electrical charges weakly or strongly sorbed in the Stern layer and electrical charges localized in a diffuse layer in which their interaction with the mineral surface is purely Coulombic in nature (Revil & Leroy 2001). The propagation of the seismic wave generates relative movements between the aqueous phase and the solid phase. The drag of the electrical charges present in the diffuse layer is responsible for a net current density in the Lagrangian framework associated with the deformation of the solid phase (Neev & Yeatts 1989; Pride 1994).

In saturated conditions, three types of seismoelectric effects are usually observed. The first is related to the seismic source itself (Mahardika *et al.* 2012). The second type of electrical field is called the coseismic electrical field and is associated with the passage of a seismic wave itself through a bipole of electrodes (Pride & Garambois 2005). This electrical field disturbance travels at the same speed than the seismic waves. The third type of electrical field corresponds to the interface seismoelectric conversion and can be remotely measured

away from this interface (Haartsen & Pride 1997). This electromagnetic disturbance is generated and remotely observed when a seismic wave passed through a sharp heterogeneity characterized by a drop in the material properties entering the coupled hydromechanical and electromagnetic problem (Martner & Sparks 1959; Dupuis *et al.* 2009). Sharp contrasts in the permeability and electrical conductivity are usually responsible for strong seismoelectric conversions.

In previous studies (for instance Haartsen & Pride 1997), the numerical modelling of the seismoelectric problem was usually performed by solving a system of partial differential equations in three steps: (1) solving the dynamic poroelastic Biot theory (Biot 1956a,b) in order to get the solid and fluid displacements vectors associated with the occurrence of seismic sources and the propagation of the seismic waves, (2) computing the source current density of electrokinetic nature associated with the drag of the charge of the electrical diffuse layer with respect to the solid phase (involving the use of the zeta potential, a key electrochemical property of the electrical double layer) and (3) solving the electromagnetic problem in the diffusive or quasi-static limits of the Maxwell equations. Various numerical methods have been employed to solve the set of the seismoelectric equations including the reflectivity method (Haartsen & Pride 1997; Garambois & Dietrich 2002); the finite differences method (Haines & Pride 2006) and the finite-elements approach (Pain *et al.* 2005; Jardani *et al.* 2009; Zyserman *et al.* 2010; Santos 2011). These studies have been developed for the fully water-saturated case only.

In partially saturated media, the saturation of the aqueous phase can affect the amplitude of the both coseismic fields and interface response signal (Strahser *et al.* 2011). Laboratory experiments, such as those conducted for instance by Parkhomenko & Gaskarov (1971) and recently by Bordes *et al.* (2008), have highlighted the increase of the amplitude of the seismoelectric coupling with increasing water saturation. In field conditions, Kullessa *et al.* (2006) showed that the coseismic wave is impacted by the water content in the vadose zone. Strahser *et al.* (2011) empirically derived the transfer equation in unsaturated conditions connecting the electrical field and seismic amplitudes. In their approach, the saturation dependence of the coseismic electrical field takes the form of a power law of the effective saturation. Haines *et al.* (2007) claim that in unsaturated conditions, the acceleration of the grains is the main term creating the electrical fields. Dupuis *et al.* (2007) used the seismoelectric method to identify the water table interface of an unconfined aquifer and to characterize saturation contrasts in the vadose zone, which can be undetectable with the seismic method alone. Butler (1996) mentioned (with no theoretical support) that the contrasts of saturation would be less likely to generate interfacial responses than the lithological contrasts. However, Revil & Mahardika (2013) and Revil *et al.* (2014) came to an opposite conclusion based on an extension of the seismoelectric model in unsaturated conditions. They proposed a seismoelectric model in unsaturated conditions and valid whatever the thickness of the double layer with respect to the size of the pores. Their model is based on the concept of effective charge density contained in the aqueous phase and can be dragged by the flow of the pore water (Jardani *et al.* 2007). This effective charge density can be in turn related directly to the permeability of the porous material to the aqueous phase (Jardani *et al.* 2007; Revil & Mahardika 2013). Also this effective charge density is defined in a dynamic sense (i.e. associated with the flow of the aqueous phase) and has nothing to do with the “static” excess charge density of the diffuse layer at rest (Revil *et al.* 2014). In parallel, Warden *et al.* (2013) extended empirically the equations developed by Pride (1994) to unsaturated media. The extension of the mechanical equations was based on a generalization of the Biot–Gassman theory to the unsaturated conditions. For the electromagnetic problem, the electrical properties such as the dielectric permittivity and the electrical conductivity were expressed as a function of the water saturation. These two formulations are valid for the unsaturated case with the second fluid phase being a non-wetting phase, very compressible, and at constant pressure.

In this paper, we use a set of coupled partial differential equations developed by Santos *et al.* (1990a) and Lo *et al.* (2005) to describe the physics involved in the wave propagation and attenuation in porous media saturated by two immiscible fluids and with a linear elastic skeleton. These equations take into account the effects of inertial coupling and changes in capillary pressure (see also related discussions in Berryman *et al.* 1988; Tuncay & Corapcioglu 1997, and Santos *et al.* 1990a,b among others). For the electromagnetic coupling, we extend the formulation developed by Revil & Mahardika (2013) and Revil *et al.* (2014) to provide a rigorous description of the electrokinetic response in two-phase flow conditions. We provide below the couplings between the seismic and electrical problems for the seismoelectric problem for which the electroosmotic effect is neglected. The partial differential equations will be solved with the finite element method. We will perform some sensitivity studies to better understand the effect of saturation on both the co-seismic electrical field and the interface response.

2 SEISMOELECTRIC THEORY IN TWO-PHASE FLOW CONDITIONS

2.1 Biot theory in two phase flow conditions

We consider below an isotropic linear poroelastic body with two Newtonian and immiscible fluid phases filling the connected pore space of the material. The propagation of seismic waves through such a porous material was presented by Lo *et al.* (2002, 2005), among others, using the continuum mechanics of mixtures. This theory was derived in an Eulerian framework. The final field equation admits four types of wave modes: three compressional (P) waves and one shear (S) wave with dissipation terms due to the momentum transfer and interaction terms between the solid and viscous Newtonian fluids phases within the porous medium. Using numerical simulations, Santos *et al.* (1990a, 2004) concluded that two of the compressional waves are analogous to the Biot fast and slow P waves in a water-saturated poroelastic material and the third P wave is a diffusive wave related to fluctuations in the capillary pressure (pressure difference between the fluid pressures of the non-wetting and wetting fluid phases).

The general elastodynamic problem consists in solving a set of coupled partial differential equations with three unknowns vectors including \mathbf{u} (the displacement vector field of the solid phase), and \mathbf{u}_1 and \mathbf{u}_2 , the displacement vector fields of the two immiscible fluid

phases 1 and 2. In the following, the non-wetting fluid corresponds to $i = 1$ (fluid 1, typically air or oil), and the wetting fluid corresponds to $i = 2$ (fluid 2). The wetting fluid is by definition the one in contact with the solid grains. Note that in carbonate rocks, the oil phase can be the wetting fluid. In the shallow subsurface, oil wettability can change from being non-wetting to wetting because of the formation of biopolymers between the oil and the solid grains. In siliciclastic reservoirs, oil can also be sorbed on the surface of clay minerals by divalent cations.

The momentum conservation equation for each fluid phase (Newton's law) is written as (Lo *et al.* 2005),

$$\rho_i \theta_i \frac{\partial^2 \mathbf{u}_i}{\partial t^2} + \theta_i \nabla p_i - R_{ii} \left(\frac{\partial \mathbf{u}_i}{\partial t} - \frac{\partial \mathbf{u}}{\partial t} \right) - \sum_{j=1}^2 A_{ij} \left(\frac{\partial^2 \mathbf{u}_j}{\partial t^2} - \frac{\partial^2 \mathbf{u}}{\partial t^2} \right) = \mathbf{0}, \quad (i = 1, 2), \quad (1)$$

while for the solid phase, the momentum conservation equation is given by

$$\rho_s \theta_s \frac{\partial^2 \mathbf{u}}{\partial t^2} + \sum_{i=1}^2 p_i \nabla \theta_i + \sum_{i=1}^2 R_{ii} \left(\frac{\partial \mathbf{u}_i}{\partial t} - \frac{\partial \mathbf{u}}{\partial t} \right) + \sum_{i=1}^2 \sum_{j=1}^2 A_{ij} \left(\frac{\partial^2 \mathbf{u}_j}{\partial t^2} - \frac{\partial^2 \mathbf{u}}{\partial t^2} \right) - \nabla \cdot \mathbf{T} = \mathbf{0}. \quad (2)$$

The stress tensor \mathbf{T} is related to the deformation of the different phases by a generalized Hookes's law,

$$\mathbf{T} = \left[\left(a_{11} - \frac{2}{3} G \right) \nabla \cdot \mathbf{u} + a_{12} \nabla \cdot \mathbf{u}_1 + a_{13} \nabla \cdot \mathbf{u}_2 \right] \mathbf{I} + 2G \mathbf{e}. \quad (3)$$

In these equations, G denotes the shear modulus of the porous medium frame (in Pa), \mathbf{I} is the 3×3 identity matrix, p_i is the fluid pressure of the fluid phases i (in Pa), A_{ij} denotes the constitutive coefficients accounting for the effect of inertial couplings, R_{ii} denotes the coefficients related to viscous drag, and ρ_i and ρ_s denote the mass density of the fluid i and the solid, respectively. The shear modulus G is the shear modulus of the skeleton since none of the two fluids can bear shear stresses.

In eqs (1) and (2), the parameter $\theta_s = 1 - \phi$ denotes the volume fraction of the solid phase, and the parameter $\theta_i = \phi S_i$ denotes the volume fraction of the i th fluid phase (ϕ , dimensionless, denotes the connected porosity and $0 \leq S_i \leq 1$ denotes the partial saturation of fluid phase i). The second-rank symmetric tensor \mathbf{T} denotes the stress tensor associated with the solid phase and a_{nm} ($n, m = 1, 2, 3$) denote the elastic coefficients with their cross-terms being symmetric, that is, $a_{nm} = a_{mn}$. The infinitesimal solid phase strain tensor of the elastic skeleton is defined by,

$$\mathbf{e} = \frac{1}{2} [\nabla \mathbf{u} + \nabla \mathbf{u}^T], \quad (4)$$

where the superscript T denotes the transpose of the matrix representing the tensor associated with the gradient of the displacement of the solid displacement.

Following the classical dynamic Biot theory for a single fluid phase saturating a linear elastic skeleton, the linear stress-strain relations for an elastic porous medium bearing two immiscible Newtonian fluids have been generalized by Tuncay & Corapcioglu (1996) using a volume-averaging approach. They obtained:

$$-\theta_1 p_1 = a_{12} \nabla \cdot \mathbf{u} + a_{22} \nabla \cdot \mathbf{u}_1 + a_{23} \nabla \cdot \mathbf{u}_2, \quad (5)$$

$$-\theta_2 p_2 = a_{13} \nabla \cdot \mathbf{u} + a_{23} \nabla \cdot \mathbf{u}_1 + a_{33} \nabla \cdot \mathbf{u}_2, \quad (6)$$

where p_1 and p_2 denote the infinitesimal changes of the non-wetting and wetting pressures, respectively (the capillary pressure is defined as $p_c = p_1 - p_2$). The two fluid pressures p_1 and p_2 are linearly connected to the volumetric strains of the solid and fluid phases. These linear constitutive relationships depend on the elastic properties of the skeleton and the properties of the two fluids as discussed below.

To simplify the previous set of equations and following Lo *et al.* (2002, 2005), we neglect the inertial drags between the two fluids (i.e. $A_{12} = A_{21} = 0$). We also introduce the average (macroscopic) filtration displacement vector of the fluid phase i relative to the solid phase:

$$\mathbf{w}_i = \theta_i (\mathbf{u}_i - \mathbf{u}). \quad (7)$$

We introduce now the filtration displacements inside the continuity and constitutive equations. For the two fluid phases, the modified momentum conservation equation obtained from eqs (1) and (7) (using $A_{12} = A_{21} = 0$) is obtained as

$$\rho_i \frac{\partial^2 \mathbf{u}}{\partial t^2} + \left(\frac{\rho_i}{\theta_i} - \frac{A_{ii}}{\theta_i^2} \right) \frac{\partial^2 \mathbf{w}_i}{\partial t^2} - \frac{R_{ii}}{\theta_i^2} \frac{\partial \mathbf{w}_i}{\partial t} = -\nabla p_i, \quad (i = 1, 2). \quad (8)$$

For the solid phase, from eqs (2) and (7), we obtain

$$\rho_s \theta_s \frac{\partial^2 \mathbf{u}}{\partial t^2} + \sum_{i=1}^2 \frac{A_{ii}}{\theta_i} \frac{\partial^2 \mathbf{w}_i}{\partial t^2} + \sum_{i=1}^2 \frac{R_{ii}}{\theta_i} \frac{\partial \mathbf{w}_i}{\partial t} = \nabla \cdot \mathbf{T}. \quad (9)$$

We use now eq. (8) to rewrite eq. (9) as:

$$\rho_T \frac{\partial^2 \mathbf{u}}{\partial t^2} + \sum_{i=1}^2 \rho_i \frac{\partial^2 \mathbf{w}_i}{\partial t^2} + \sum_{i=1}^2 \theta_i \nabla p_i = \nabla \cdot \mathbf{T}, \quad (10)$$

where the expression of the stress tensor acting on the solid phase is given from eq. (3) as

$$\mathbf{T} = \left[\left(\bar{a}_{1s} - \frac{2}{3}G \right) \nabla \cdot \mathbf{u} + \frac{a_{12}}{\theta_1} \nabla \cdot \mathbf{w}_1 + \frac{a_{13}}{\theta_2} \nabla \cdot \mathbf{w}_2 \right] \mathbf{I} + 2G\mathbf{e}, \quad (11)$$

with

$$\bar{a}_{1s} = a_{11} + a_{12} + a_{13}, \quad (12)$$

and where $\rho_T = \rho_s(1 - \phi) + \rho_1\theta_1 + \rho_2\theta_2$ denotes the averaged mass density of the fluid–solid mixture, that is, the mass density of the porous body. The material properties entering eqs (8)–(11) have been derived by Lo *et al.* (2005) as:

$$a_{11} = K_s(1 - \phi - \delta_s), \quad (13)$$

with

$$a_{12} = a_{12} = -K_s\delta_1 \quad (14)$$

$$a_{13} = a_{31} = -K_s\delta_2 \quad (15)$$

$$a_{22} = -\frac{1}{M_1} \left[\left(K_1K_2 \frac{dS_1}{dp_c} + \frac{K_1K_2S_1}{1-S_1} \frac{dS_1}{dp_c} + K_1S_1 \right) \delta_1 + \frac{K_1K_2\phi S_1}{1-S_1} \frac{dS_1}{dp_c} + K_1S_1\phi \right], \quad (16)$$

$$a_{23} = a_{32} = -\left[\frac{\delta_1\delta_2}{\delta_s} K_s + \frac{K_1K_2\phi}{M_1} \frac{dS_1}{dp_c} \right] \quad (17)$$

$$a_{22} = -\frac{1}{M_1} \left[\left(K_1K_2 \frac{dS_1}{dp_c} + \frac{K_1K_2(1-S_1)}{S_1} \frac{dS_1}{dp_c} + K_2(1-S_1) \right) \delta_2 + \frac{K_1K_2\phi(1-S_1)}{S_1} \frac{dS_1}{dp_c} + K_1(1-S_1)\phi \right] \quad (18)$$

$$R_{11} = -\frac{\theta_1\eta_1}{k_s k_{r1}}, \quad (19)$$

$$R_{22} = -\frac{\theta_2\eta_2}{k_s k_{r2}}, \quad (20)$$

$$A_{11} = (1 - \alpha_s) \rho_1 \theta_1, \quad (21)$$

$$A_{22} = (1 - \alpha_s) \rho_2 \theta_2, \quad (22)$$

$$\delta_s = \frac{\left(1 - \phi - \frac{K_b}{K_s} \right) K_s}{K_s + \frac{M_1}{M_2} \left(\frac{K_b}{K_s} + \phi - 1 \right)}, \quad (23)$$

$$\delta_1 = -\frac{K_1 \left(S_1 + K_2 \frac{dS_1}{dp_c} + \frac{K_2 S_1}{1-S_1} \frac{dS_1}{dp_c} \right) \left(1 - \phi - \frac{K_b}{K_s} \right)}{K_s M_1 + M_2 \left(\frac{K_b}{K_s} + \phi - 1 \right)}, \quad (24)$$

$$\delta_2 = \frac{K_2 \left(1 - S_1 + \frac{K_1}{S_1} \frac{dS_1}{dp_c} \right) \left(1 - \phi - \frac{K_b}{K_s} \right)}{K_s M_1 + M_2 \left(\frac{K_b}{K_s} + \phi - 1 \right)}, \quad (25)$$

$$M_1 = -\left(\frac{K_1}{S_1} \frac{dS_1}{dp_c} + \frac{K_2}{(1-S_1)} \frac{dS_1}{dp_c} + 1 \right), \quad (26)$$

$$M_2 = \left(\frac{K_1 K_2}{\phi S_1 (1 - S_1)} \frac{dS_1}{dp_c} + \frac{K_1 S_1}{\phi} + \frac{K_2 (1 - S_1)}{\phi} \right), \quad (27)$$

where K_s (Pa) denotes the bulk modulus of solid phase; K_1 (Pa) is bulk modulus of the non-wetting fluid phase, K_2 (Pa) is the bulk modulus of the wetting fluid phase, $S_1 = \theta_1/\phi$ (dimensionless) is the relative saturation of the non-wetting fluid, η_i (Pa s) is the dynamic viscosity of the Newtonian pore fluid phase i , k_s (in m^2) is the permeability of the medium and k_{ri} (dimensionless) is the relative permeability of fluid phase i (assumed to be essentially a function of the saturation of each phase as discussed below). The term a_s (dimensionless) is defined as the bulk tortuosity of the connected pore space and therefore, the ratio a_s/ϕ denotes the electrical formation factor F (dimensionless), which can be related to the porosity by Archie's law $F = \phi^{-m}$ where $m \geq 1$ denotes the so-called cementation or porosity exponent (also called the first Archie's exponent).

Eqs (19) and (20) provide classical formulations to infer the viscous coefficients R_{11} and R_{22} of the two fluids obeying Darcy's law. In this paper, we use the van Genuchten (1980) approach to provide consistent approximations for the capillary pressure curve (dp_c/dS_1) (neglecting hysteresis for small pressure fluctuations) and to describe the saturation dependence of the relative permeabilities:

$$\frac{dp_c}{dS_1} = \frac{\rho_2 g}{m_v n_v \chi} \left((1 - S_1)^{-\frac{n_v}{n_v-1}} - 1 \right)^{\frac{1-n_v}{n_v}} (1 - S_1)^{-\left(\frac{2n_v-1}{n_v-1}\right)}, \quad (28)$$

$$k_{r1}(S_2) = (1 - S_2)^\lambda \left(1 - (S_2)^{\frac{1}{m_v}} \right)^{2m_v}, \quad (29)$$

$$k_{r2}(S_2) = (S_2)^\lambda \left(1 - \left[1 - (S_2)^{\frac{1}{m_v}} \right]^{m_v} \right)^{2m_v}, \quad (30)$$

where $m_v = 1 - 1/n_v$, n_v , χ and λ are the van Genuchten parameters (van Genuchten 1980).

2.2 The u-p formulation extended to two-phase flow problems

The classical formulation described above, eqs (8)–(10), is based on solving the partial differential equations for three unknown fields, \mathbf{u} (the solid displacement field) and \mathbf{w}_1 and \mathbf{w}_2 corresponding to the two filtration displacement vectors. For a two-dimensional discretized problem needed to solve the hydromechanical problem of wave propagation, there are therefore six degrees of freedom per node (3 vectors and two components per vector). In order to simplify the writing of the set of equations, and then its solving, we introduce below an alternative and new formulation in which we use only the displacement \mathbf{u} of the solid phase and the fluid pressures p_i as unknowns instead of the displacement/filtration vectors. This implies four unknown parameters (two components for the displacement u_1 and u_2 , and two fluid pressures p_i) to solve at each node. This approach, followed in one of our previous paper for the saturated case (Jardani *et al.* 2009), decreases substantially the overall computational effort. Note that in 3-D, the number of unknown per node would drop from 9 to 5, making the new formulation even more attractive than in 2-D.

The technique first consists in applying the Fourier transform to the set of equation described above and then to conduct some algebraic manipulations to replace the filtration displacements of the two fluid phases by their fluid pressures. We start with reformulating eq. (8), that is, the momentum conservation equations for the two fluids, in the frequency domain:

$$-\omega^2(\rho_i \mathbf{u} + \tilde{\rho}_i \mathbf{w}_i) + j\omega \frac{R_{ii}}{\theta_i^2} \mathbf{w}_i = -\nabla p_i, \quad (31)$$

where ω and j denotes the pulsation frequency and the pure imaginary number ($j^2 = -1$), respectively, and the terms $\tilde{\rho}_i$ denote the inertial drag interactions terms between the solid and fluid phases (apparent or effective densities). Note that we avoid using specific notations for the Fourier transform of the fields in order to avoid to use heavy notations. The apparent densities involved in eq. (31) are defined by

$$\tilde{\rho}_i = \left(\frac{\rho_i}{\theta_i} - \frac{A_{ii}}{\theta_i^2} \right). \quad (32)$$

Eq. (31) can be used to express the filtration displacement of each fluid phase, \mathbf{w}_i , as a function of the pore fluid pressure p_i and the displacement of the solid phase \mathbf{u} . This yields the following Darcy's equations

$$\dot{\mathbf{w}}_i = -k_i(\omega)(\nabla p_i - \omega^2 \rho_i \mathbf{u}), \quad (33)$$

in which we have,

$$k_i(\omega) = -\frac{1}{j\omega \tilde{\rho}_i + \frac{R_{ii}}{\theta_i^2}}. \quad (34)$$

Eq. (33) can also be written as $\mathbf{w}_i = \tilde{k}_i(\nabla p_i - \omega^2 \rho_i \mathbf{u})$ where $k_i(\omega)$ is the frequency-dependent apparent permeability similar to the one defined in Jardani *et al.* (2009) for the seismoelectric problem in saturated conditions, k_ω . These terms should not be confused with the permeability itself. We introduce the following quantities,

$$\tilde{k}_i = \frac{k_i(\omega)}{j\omega} = \frac{1}{\omega^2 \tilde{\rho}_i - j\omega \frac{R_{ii}}{\theta_i^2}}. \quad (35)$$

For the solid phase, the momentum conservation equation is written as,

$$-\omega^2 \left(\rho_T \mathbf{u} + \sum_{i=1}^2 \rho_i \mathbf{w}_i \right) + \sum_{i=1}^2 \theta_i \nabla p_i = \nabla \cdot \mathbf{T}. \quad (36)$$

We are going now to remove the model vectors \mathbf{w}_i from the system of partial differential equations. The momentum conservation equations for the non-wetting and wetting fluid phases are given, from eq. (31), by,

$$-\omega^2 (\rho_1 \mathbf{u} + \tilde{\rho}_1 \mathbf{w}_1) + j\omega \frac{R_{11}}{\theta_1^2} \mathbf{w}_1 = -\nabla p_1, \quad (37)$$

$$-\omega^2 (\rho_2 \mathbf{u} + \tilde{\rho}_2 \mathbf{w}_2) + j\omega \frac{R_{22}}{\theta_2^2} \mathbf{w}_2 = -\nabla p_2, \quad (38)$$

respectively. For the solid phase, the momentum conservation equation (Newton's law) is derived from eq. (36) in the frequency domain as

$$-\omega^2 (\rho_T \mathbf{u} + \rho_1 \mathbf{w}_1 + \rho_2 \mathbf{w}_2) + \theta_1 \nabla p_1 + \theta_2 \nabla p_2 = \nabla \cdot \mathbf{T}, \quad (39)$$

($i = 1, 2$), where the total stress tensor is given by eq. (11). Following the work of Biot (1962) in the saturated case, we can express the stress-strain relationships in an isotropic porous medium as:

$$-\theta_1 p_1 = a_{2s} \nabla \cdot \mathbf{u} + \frac{a_{22}}{\theta_1} \nabla \cdot \mathbf{w}_1 + \frac{a_{23}}{\theta_2} \nabla \cdot \mathbf{w}_2, \quad (40)$$

$$-\theta_2 p_2 = a_{3s} \nabla \cdot \mathbf{u} + \frac{a_{23}}{\theta_1} \nabla \cdot \mathbf{w}_1 + \frac{a_{33}}{\theta_2} \nabla \cdot \mathbf{w}_2. \quad (41)$$

These two equations can be combined to provide the expressions for the divergence of the filtration displacements for the two fluids as,

$$\nabla \cdot \mathbf{w}_1 = \alpha_{s1} \nabla \cdot \mathbf{u} + M_{11} p_1 - M_{12} p_2, \quad (42)$$

$$\nabla \cdot \mathbf{w}_2 = \alpha_{s2} \nabla \cdot \mathbf{u} - M_{12} p_1 + M_{22} p_2. \quad (43)$$

The expressions of the material properties entering eqs (43) and (44) are defined below.

In summary, we are now in the position to rewrite the equations of motion in terms of the unknown fields (\mathbf{u} , p_1 and p_2) as:

$$-\omega^2 \tilde{\rho}_T \mathbf{u} + \tilde{\theta}_1 \nabla p_1 + \tilde{\theta}_2 \nabla p_2 = \nabla \cdot \hat{\mathbf{T}}, \quad (44)$$

$$\hat{\mathbf{T}} = \bar{\lambda}_s (\nabla \cdot \mathbf{u}) \mathbf{I} + G [\nabla \mathbf{u} + \nabla \mathbf{u}^T], \quad (45)$$

$$M_{11} p_1 - \nabla \cdot \{ \tilde{k}_1 [\nabla p_1 - \omega^2 \rho_1 \mathbf{u}] \} = M_{12} p_2 - \bar{\alpha}_{s1} \nabla \cdot \mathbf{u}, \quad (46)$$

$$M_{22} p_2 - \nabla \cdot \{ \tilde{k}_2 [\nabla p_2 - \omega^2 \rho_2 \mathbf{u}] \} = M_{12} p_1 - \bar{\alpha}_{s2} \nabla \cdot \mathbf{u}. \quad (47)$$

Eq. (44) corresponds to Newton's law applied to the solid skeleton of the porous material. This equation is similar to Newton's equation of linear elastic bodies (no pores) except for the coupling terms $\tilde{\theta}_i \nabla p_i$. These coupling terms represent the viscous couplings between the solid and fluid phases. The (effective) stress tensor defined by eq. (45) corresponds to the stress acting on the solid phase if the pore fluid is replaced by vacuum. Eqs (46) and (47) are non-linear diffusion equations for the two pore fluid pressures of each fluid in which the effect of the compression of the solid phase on the pore fluid pressure and the hydraulic pressure exercised mutually between the two fluids are taken into account. As already discussed above, the two fluid pressures are related to each other by the capillary pressure curve.

The parameters entering eqs (44) to (47), as well as in eqs (42) and (43), are given by:

$$\bar{\lambda}_s = \left(\bar{a}_{1s} + \frac{a_{12}}{\theta_1} \bar{\alpha}_{s1} + \frac{a_{13}}{\theta_2} \bar{\alpha}_{s2} - \frac{2}{3} G \right), \quad (48)$$

$$\tilde{k}_i = \frac{k_i(\omega)}{j\omega} = \frac{1}{\omega^2 \tilde{\rho}_i - j\omega \frac{R_{il}}{\theta_i^2}}, \quad (49)$$

$$\tilde{\rho}_T = \rho_T - \omega^2 \rho_1^2 \tilde{k}_1 - \omega^2 \rho_2^2 \tilde{k}_2, \quad (50)$$

$$\tilde{\theta}_1 = -\alpha_{s1} - \omega^2 \rho_1 \tilde{k}_1 \quad (51)$$

$$\tilde{\theta}_2 = -\alpha_{s2} - \omega^2 \rho_2 \tilde{k}_2, \quad (52)$$

$$\alpha_{s1} = \frac{(\bar{a}_{2s}a_{33} - \bar{a}_{3s}a_{23})\theta_1}{(a_{23}^2 - a_{33}a_{22})}, \quad (53)$$

$$\alpha_{s2} = \frac{(\bar{a}_{3s}a_{22} - \bar{a}_{2s}a_{23})\theta_2}{(a_{23}^2 - a_{33}a_{22})}, \quad (54)$$

$$M_{11} = \frac{a_{33}\theta_1^2}{(a_{23}^2 - a_{33}a_{22})}, \quad (55)$$

$$M_{12} = \frac{a_{23}\theta_1\theta_2}{(a_{23}^2 - a_{33}a_{22})}, \quad (56)$$

$$M_{22} = \frac{a_{22}\theta_2^2}{(a_{23}^2 - a_{33}a_{22})}, \quad (57)$$

$$\bar{a}_{1s} = a_{11} + a_{12} + a_{13}, \quad (58)$$

$$\bar{a}_{2s} = a_{12} + a_{22} + a_{23}, \quad (59)$$

$$\bar{a}_{3s} = a_{13} + a_{23} + a_{33}. \quad (60)$$

In these equations $\tilde{\theta}_1$ and $\tilde{\theta}_2$ denote the volumetric hydromechanical coupling coefficients of the each fluid; $\bar{\lambda}_s$ is the Lamé modulus of the solid phase (in Pa); \tilde{k}_1 and \tilde{k}_2 are the dynamic permeability of the each fluid (in m²), $\tilde{\rho}_T$ (in m³ kg⁻¹) is an apparent mass density for the solid phase at a given frequency ω and finally M_{11} and M_{22} denote two storativity coefficients of the porous body.

2.3 Seismoelectric conversions in two phase flow conditions

For describing the electromagnetic response in the quasi-static limit of the Maxwell equations, we consider that the interfaces/heterogeneities are close enough (few hundred meters at most) from the electromagnetic sensors (pair of electrodes, antennas, magnetometers) to neglect the time required by the electromagnetic disturbances to diffuse between the two. We have already demonstrated the validity of this approximation in several of our previous papers (e.g. Araj *et al.* 2012). In this case, we can model the problem by solving only the quasi-static electromagnetic problem using a Poisson equation for the electrical potential as discussed below.

The seismoelectric signal is due to the relative displacement of the fluids generated by a seismic source and the existence of an electrical double layer at the interface between the different phases of the porous composite (Revil *et al.* 1999). We already know that the solid water interface is typically charged as shown for instance in Fig. 1 for silica. The charge on the mineral surface is counterbalanced by counterions located in the diffuse and Stern layer and co-ions located in the diffuse layer.

In multiphase flow conditions, we should also consider that the interface between the two fluids can be charged. For instance, we know from electrokinetic measurements (e.g. electrophoretic mobility measurements of gas bubbles) that the air water interface is charged (Fig. 2) (see for instance Leroy *et al.* 2012, for a complete model of this electrical double layer). The oil water interface is also charged especially when the oil is the wetting phase. In this case, the oil is expected to be rich in polymers such as resins and asphaltens, which can generate a conductive gel later at the oil water interface (see fig. 3 and discussion in Alkafef *et al.* 2001; Revil & Jardani 2010).

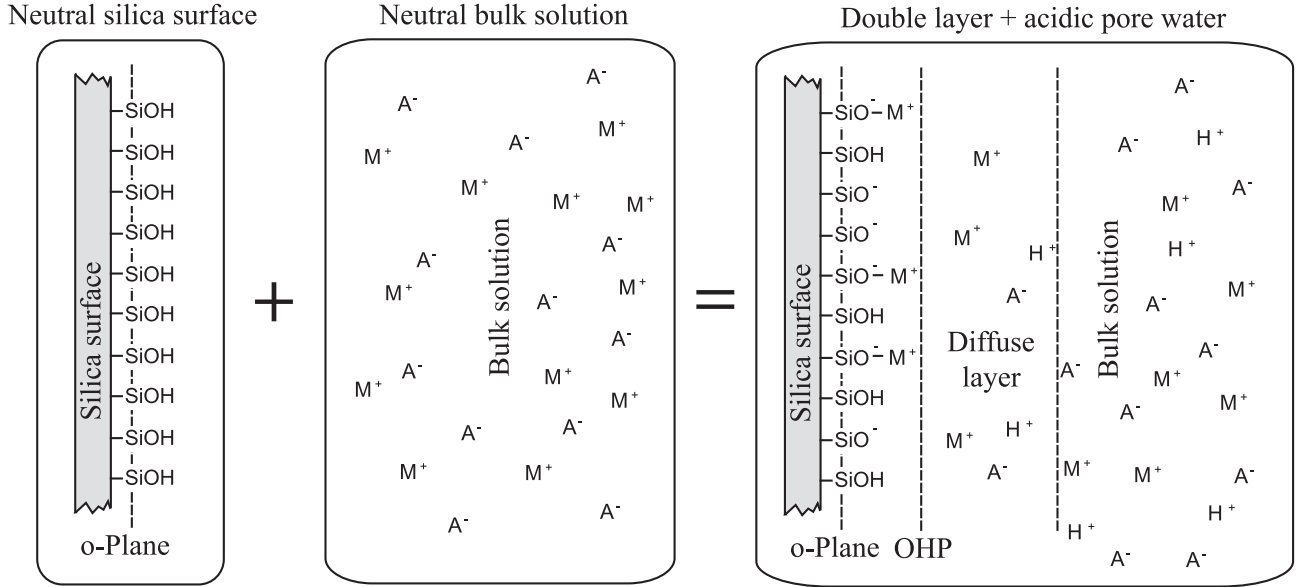


Figure 1. Electrical double layer at the solid pore water interface. Formation of the electrical double layer in the case of a silica surface brought in contact with a neutral pore water composed of cations (M^+) and anions (A^-). The silanol surface groups at the surface of silica $>Si-OH$ release a certain number of protons in the pore water making the solution more or less acidic depending on the surface area per pore volume ratio and the surface of the mineral negatively charged (with $>Si-O^-$ surface sites). Some of the cations from the pore water are adsorbed in the Stern layer, the inner portion of the electrical double layer. The surface charge density and the Stern layer charge density are compensated in the diffuse layer by an excess of counterions. In a sandstone, the bulk pore water is neutral (no net charge density) and only the diffuse layer is not neutral and more usually characterized by an excess of (positive) charges. The drag of this charge density is responsible for the streaming current density, which acts as a source in the Maxwell equations.

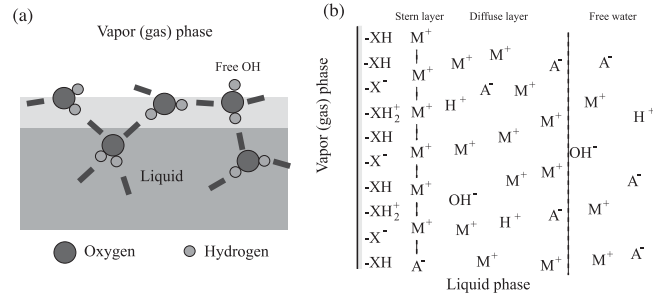


Figure 2. Electrical double layer at the air water interface. (a) First two water layers with their hydrogen bonding network at the interface between the vapour phase (air) and the liquid water phase according to Tarbuck *et al.* (2006). The topmost water layer is a thin depletion layer. In this layer, the water dipoles are oriented slightly into the bulk and possess ‘free’ dangling hydroxyl sites $>OH$. The water molecules located in this depletion layer have fewer and weaker hydrogen bonding interactions than the tri- and tetrahedrally coordinated water molecules located in the second layer where hydrogen atoms point preferentially towards the liquid water phase. (b) Electrical double layer model at the interface between the vapour phase and the liquid water phase in the case of a binary monovalent electrolyte with M^+ represents the metal cations and A^- the anions.

The electric problem is coupled to the hydromechanical equations via the current density term that is co-linear with the relative velocities of the two fluid phases with respect to the solid phase (filtration velocities). Extending the approach developed by Jardani *et al.* (2009) for the saturated case to the two phase flow conditions, the electric problem can be written in the frequency domain as (see Appendix A):

$$\nabla \cdot (\sigma \nabla \psi) = \nabla \cdot \mathbf{J}_S, \quad (61)$$

$$\mathbf{J}_S = \frac{\hat{Q}_1^0}{S_1} \dot{\mathbf{w}}_1 + \frac{\hat{Q}_2^0}{S_2} \dot{\mathbf{w}}_2, \quad (62)$$

$$\mathbf{J}_S = -j\omega \frac{\hat{Q}_1^0}{S_1} \tilde{k}_1 (\nabla p_1 - \omega^2 \rho_1 \mathbf{u}) - j\omega \frac{\hat{Q}_2^0}{S_2} \tilde{k}_2 (\nabla p_2 - \omega^2 \rho_2 \mathbf{u}), \quad (63)$$

where ψ (in V) is the electrostatic potential, the electrical field \mathbf{E} (in $V\ m^{-1}$) is given by $\mathbf{E} = -\nabla \psi$ in the quasi-static limit of the Maxwell equations for which $\nabla \times \mathbf{E} = 0$, σ (in $S\ m^{-1}$) is the electrical conductivity of the porous medium, and \mathbf{J}_S (in $A\ m^{-2}$) is the source current density of electrokinetic nature produced by the relative motion between the fluids and the solid phase. The effective charge densities \hat{Q}_1^0 and

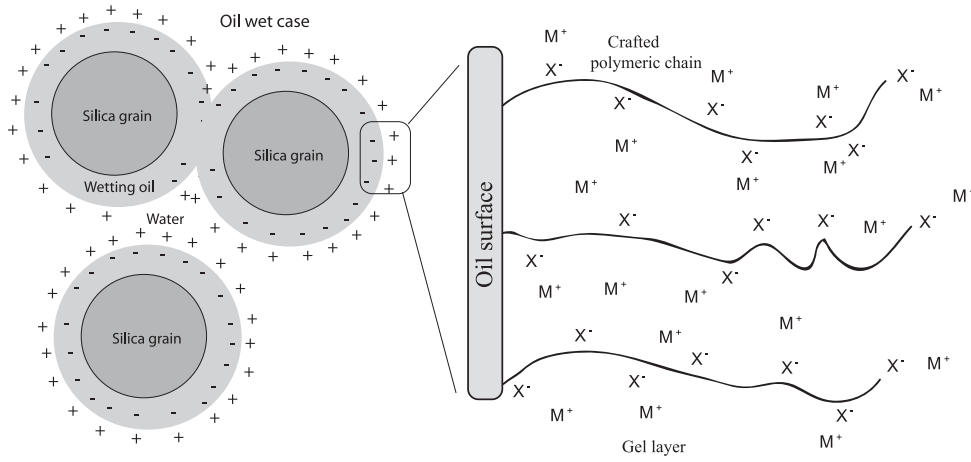


Figure 3. Surface charge and conductive gel in presence of a wetting oil rich in resins and asphaltens. This components makes the oil being a solvent and there are responsible for the formation of an electrical double layer at the oil water interface. This oil water interface is associated with the formation of protuding polymers into the water phase. The negative sites X^- corresponds to the $R-COO^-$ site of the polar polymers negatively charged. M^+ corresponds to the counterions (the anions A^- are not shown here). Note that the oil is therefore surrounded by a conductive shell corresponding to a gel with a strong excess of counterions.

\hat{Q}_2^0 denote the effective excess of charge (of the diffuse layer) per unit pore volume (expressed in $C\ m^{-3}$) of the non-wetting and wetting fluid phases, respectively (Appendix A).

For most cases of interest, the non-wetting phase will be also an electrical insulating phase (e.g. air or oil) and therefore we can assume that its excess of charge \hat{Q}_1^0 is vanishingly small or null. In this case, we write the source current density as (Appendix A):

$$\mathbf{J}_S \approx -j\omega \frac{\hat{Q}_2^0}{S_2} \tilde{k}_2 (\nabla p_2 - \omega^2 \rho_2 \mathbf{u}). \quad (64)$$

With the same assumptions, the electrical conductivity of the porous material can be written as (e.g. Waxman & Smits 1968; Revil 2013a,b; Revil *et al.* 2014)

$$\sigma = \frac{1}{F} S_2^n \sigma_f + \frac{1}{F\phi} S_2^{n-1} \sigma_s, \quad (65)$$

where σ_f (in $S\ m^{-1}$) denotes the pore water conductivity, F denotes the formation factor introduced above (ratio of the pore space tortuosity to the connected porosity), n (dimensionless) is the second Archie's exponent and σ_s ($S\ m^{-1}$) denotes the surface conductivity associated with the existence of the electrical double layer coating the surface of the different phases. Revil (2013a) provided an expression to connect its surface conductivity to the tortuosity of the pore network and to the cation exchange capacity of the material.

The effect of the water saturation on the excess of electrical charges per unit volume is taken into account by extending the relationship between these two parameters in unsaturated conditions shown in Fig. 4 (see Linde *et al.* 2007; Revil *et al.* 2007). This approach seems valid in both saturated and unsaturated conditions (see discussion in Jounnot & Linde 2013).

3 NUMERICAL SIMULATIONS OF THE SEISMOELECTRIC THEORY

3.1 The effect of the water content on the coseismic disturbance

Pride & Haartsen (1996) proposed a relationship of proportionality between the electrical fields and the acceleration of the grains. This proportionality was observed in the set of the seismic and seismoelectric data conducted in the field by Garambois & Dietrich (2001). In fully water-saturated conditions, the transfer function for the coseismic electrical disturbance associated with the P wave was derived from the eigenvalue response of an isotropic and homogenous medium and is given by:

$$\frac{\mathbf{E}}{-\omega^2 \mathbf{u}} = -\frac{\rho_2 \varepsilon_2 \zeta}{\sigma_f \mu_2} \left(1 - \frac{\rho}{\rho_2} \frac{C}{H} \right), \quad (66)$$

where \mathbf{E} and \mathbf{u} are the electrical field and solid phase displacement, respectively, ε_2 is the dielectric permittivity of the aqueous phase, μ_2 is its viscosity and ζ denotes the zeta potential (in V) and where C and H are elastic moduli in Pa (as defined by Biot 1962) and related to the undrained bulk modulus K_u (Pa) and Skempton's coefficient B (dimensionless) by

$$C = BK_u, \quad (67)$$

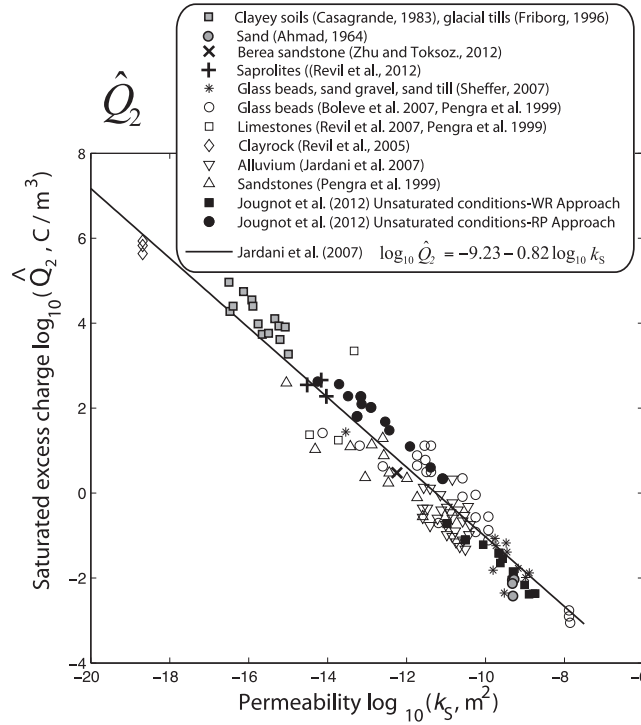


Figure 4. Quasi-static charge density \hat{Q}_2^0 versus the quasi-static permeability for a broad collection of core samples and porous materials. This charge density is derived directly from the streaming potential coupling coefficient using eq. (92). Data from Ahmad (1964), Bolève *et al.* (2007), Casagrande (1983), Friborg (1996), Jougnot *et al.* (2012), Jardani *et al.* (2007), Pengra *et al.* (1999), Revil *et al.* (2005, 2007), Sheffer (2007); Revil (2012) and Zhu & Toksöz (2012). All the data correspond to the water-saturated case except for those from Jougnot *et al.* (2012).

$$H = K_u + \frac{4}{3}G. \quad (68)$$

Eq. (66) connects the various physical properties to the amplitudes of coseismic electric fields that travel along with seismic P wave.

In this section, our goal is to extend eq. (66) to a porous medium saturated with two immiscible fluids phases. Following Garambois & Dietrich (2001) for the saturated case, we consider a 1-D compressional pure harmonic plane wave in a homogenous and isotropic material.

$$\mathbf{u} = U \exp[j(kx - \omega t)] \hat{\mathbf{x}}, \quad (69)$$

$$\mathbf{w}_1 = W_1 \exp[j(kx - \omega t)] \hat{\mathbf{x}}, \quad (70)$$

$$\mathbf{w}_2 = W_2 \exp[j(kx - \omega t)] \hat{\mathbf{x}}, \quad (71)$$

$$\mathbf{E} = E \exp[j(kx - \omega t)] \hat{\mathbf{x}}, \quad (72)$$

where U , W_1 and W_2 are wave amplitudes, $\hat{\mathbf{x}}$ is the unit vector in the wave propagation direction, ω is the angular wave excitation frequency, $k = k_r + jk_i$ is a complex wave number that includes attenuation coefficient (the phase slowness can be defined as $s = k_r/\omega$). The complete set of governing equations describing the poroelastic problem (eqs 8–11) can be reduced of three vector equations as follow:

$$\left\{ -\omega^2 \begin{bmatrix} \rho_s \theta_s & \frac{A_{11}}{\theta_1} & \frac{A_{22}}{\theta_2} \\ \rho_1 \theta_1 & \tilde{\rho}_1 \theta_1 & 0 \\ \rho_2 \theta_2 & 0 & \tilde{\rho}_2 \theta_2 \end{bmatrix} + j\omega \begin{bmatrix} 0 & -\frac{R_{11}}{\theta_1} & -\frac{R_{22}}{\theta_2} \\ 0 & \frac{R_{11}}{\theta_1} & 0 \\ 0 & 0 & \frac{R_{22}}{\theta_1} \end{bmatrix} + k^2 \begin{bmatrix} \tilde{a}_{11} & \frac{a_{12}}{\theta_1} & \frac{a_{13}}{\theta_2} \\ a_{2s} & \frac{a_{22}}{\theta_1} & \frac{a_{23}}{\theta_2} \\ a_{3s} & \frac{a_{23}}{\theta_1} & \frac{a_{33}}{\theta_2} \end{bmatrix} \right\} \begin{bmatrix} U \\ W_1 \\ W_2 \end{bmatrix} = \begin{bmatrix} 0 \\ 0 \\ 0 \end{bmatrix}. \quad (73)$$

The existence of a solution to eq. (73) requires that the determinant of the matrix indicated in curly brackets must vanish (Vasco & Minkoff 2012). The determinant can be formulated as:

$$Q_3 \tau^3 + Q_2 \tau^2 + Q_1 \tau + Q_0 = 0, \quad (74)$$

Table 1. Petrophysical properties used to solve the seismic problem for the synthetic case study.

Property	Symbol	Value
Bulk modulus of air	K_1 (MPa)	0.145
Bulk modulus (drained)	K_b (GPa)	1.02
Bulk modulus of solid	K_s (GPa)	35
Bulk modulus of water	K_2 (GPa)	2.25
Fitting parameter	n_v (—)	2.03
Fitting parameter	β_v	0.5
Fitting parameter	χ (—)	2.39
Material density of air	ρ_1 (kg m ⁻³)	1.1
Material density of solid	ρ_s (kg m ⁻³)	2650
Material density of water	ρ_2 (kg m ⁻³)	997
Permeability	k (m ²)	10 ⁻¹²
Porosity	ϕ (—)	0.23
Shear modulus	G (GPa)	1.44
Viscosity of air	β_1 (N s m ⁻²)	18 × 10 ⁻⁶
Viscosity of water	β_2 (N s m ⁻²)	0.001
Pore water conductivity	σ_f (S m ⁻¹)	0.1
Surface conductivity	σ_s (S m ⁻¹)	10 ⁻³

with $\tau = k^2$. For a given frequency, the polynomial of eq. (74) of the dispersion has three complex roots and the wave number has six roots (see details in Appendix B). However, only three of these roots are physically possible (see Tuncay & Corapcioglu 1996). This implies the existence of three compressional waves in a poroelastic medium saturated by two immiscible fluids.

According to the numerical analysis conducted by Vasco & Minkoff (2012, see also Tuncay & Corapcioglu 1996; Santos *et al.* 1990a; Santos *et al.* 2004; Lo *et al.* 2005), the P1 and P2 waves correspond to the fast and slow compressional waves of the classical dynamic Biot's model (Biot 1962) in saturated conditions. The third wave (P3) is a diffusive wave due to the pressure fluctuations between the two fluid phases and its phase speed depends on the slope of the capillary pressure with the saturation of the wetting phase (Lo *et al.* 2005).

We solved the polynomial eq. (74) in the low frequency regime (10 Hz) for the air–water mixture to study the effect of the water saturation on the velocity of the three wave modes using the value of the poroelastic parameters given in Table 1. The result is shown in Fig. 5. At low saturations, the wave velocity of the (fast) P1 wave decreases with water saturation because the total density increases with the saturation (Whitman & Towle 1992; Lo *et al.* 2005). At very high water saturation, the compressional velocity is controlled by the fluid bulk modulus H rather than by the bulk density and therefore increases sharply with the saturation near full saturation (Fig. 5). The velocity of the P1 wave at low frequencies can be approximately determined by (e.g. Lo *et al.* 2005):

$$c_{pI} \approx \sqrt{\frac{H}{\rho_T}}, \quad (75)$$

where

$$H = \tilde{a}_{11} + a_{22} + a_{33} + 2(a_{12} + a_{13} + a_{23}). \quad (76)$$

The second dilatational wave (P2 wave) propagates as a diffusion wave (Biot 1956a,b; Santos *et al.* 1990a; Tuncay & Corapcioglu 1996) while the third mode of propagation (P3 wave characterized by the lowest velocity among the three types of waves), occurs from the pressure difference between the two fluid phases. Therefore, the mode P3 does not exist in fully-water saturated conditions.

The attenuation coefficients derived from the imaginary part of the phase velocity for the three modes are shown in Fig. 6. It is seen that the attenuation increases with water saturation for the P1 wave. Because of the strong attenuation of the P2 and P3 waves, the experimental detection of these waves is extremely difficult (Figs 5 and 6 call for more details on the behaviours observed).

We now reformulate the amplitude of the relative displacement of the fluid phases W_1 and W_2 as a function of the amplitude of the solid phase U . After some algebraic manipulations, we obtain for the three types of compressional waves

$$\mathbf{w}_1 = \beta_{p_1, p_2, p_3}^I U \exp[j(kx - \omega t)] \hat{\mathbf{x}} \quad (77)$$

$$\mathbf{w}_2 = \beta_{p_1, p_2, p_3}^{II} U \exp[j(kx - \omega t)] \hat{\mathbf{x}}, \quad (78)$$

where

$$\beta_{p_1, p_2, p_3}^I = \frac{(s_{p_1, p_2, p_3}^2 a_{2s} - \rho_1 \theta_1) \left(s_{p_1, p_2, p_3}^2 \frac{a_{13}}{\theta_2} - \Gamma_2 \right) - (s_{p_1, p_2, p_3}^2 \tilde{a}_{11} - \rho_s \theta_s) \frac{a_{23}}{\theta_2} s_{p_1, p_2, p_3}^2}{\frac{a_{23}}{\theta_2} s_{p_1, p_2, p_3}^2 \left(s_{p_1, p_2, p_3}^2 \frac{a_{12}}{\theta_1} - \Gamma_1 \right) - \left(s_{p_1, p_2, p_3}^2 \frac{a_{22}}{\theta_1} - \Lambda_1 \right) \left(s_{p_1, p_2, p_3}^2 \frac{a_{13}}{\theta_2} - \Gamma_2 \right)}, \quad (79)$$

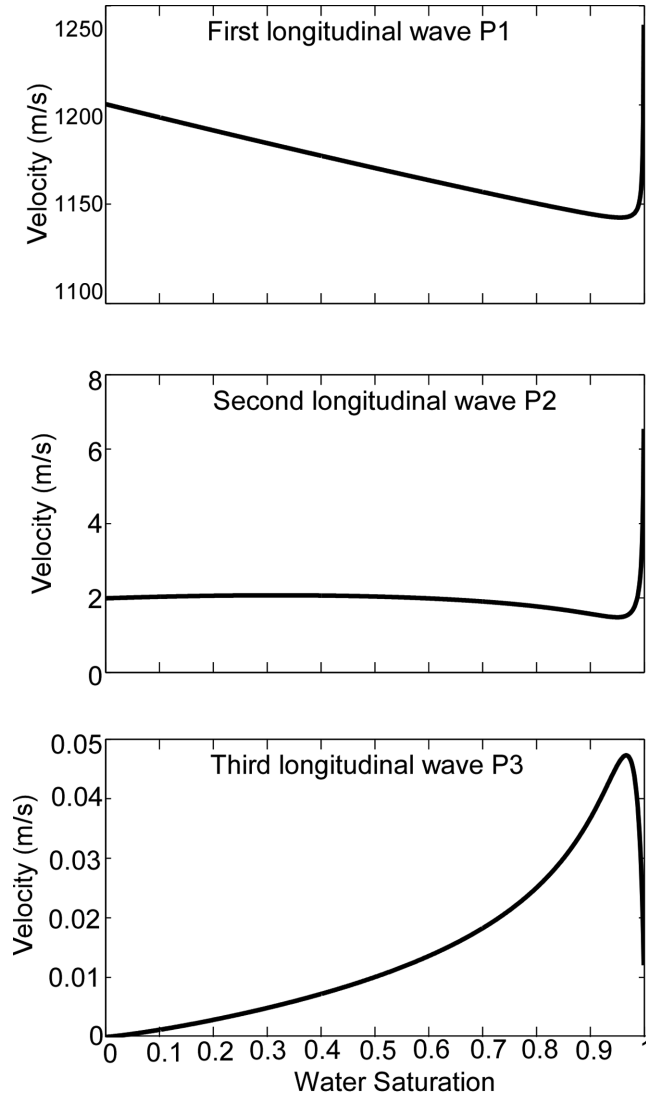


Figure 5. Effect of water saturation on the three phase velocities of the longitudinal modes propagation wave derived from the real component of the roots of cubic eq. (74) at a frequency of 10 Hz used in the compute (material properties from Table 1). The velocity of the first wave decreases when water saturation increases, due to an increase of bulk density and an increase of the bulk modulus near full saturation produces a raise of the velocity. The second dilatational wave (P2 wave) propagates is a diffusion wave with a velocity arising in the fully saturated condition. The third wave occurs from the pressure difference between the fluid phases. Then, when only one fluid occupies the pore space, the phase velocity vanishes.

$$\beta_{p_1, p_2, p_3}^{II} = \frac{(s_{p_1, p_2, p_3}^2 a_{2s} - \rho_1 \theta_1) (s_{p_1, p_2, p_3}^2 \frac{a_{12}}{\theta_1} - \Gamma_1) - (s_{p_1, p_2, p_3}^2 \tilde{a}_{11} - \rho_s \theta_s) (s_{p_1, p_2, p_3}^2 \frac{a_{22}}{\theta_1} - \Lambda_1)}{(s_{p_1, p_2, p_3}^2 \frac{a_{22}}{\theta_1} - \Lambda_1) (s_{p_1, p_2, p_3}^2 \frac{a_{13}}{\theta_2} - \Gamma_2) - (s_{p_1, p_2, p_3}^2 \frac{a_{12}}{\theta_1} - \Gamma_1) \frac{a_{23}}{\theta_2} s_{p_1, p_2, p_3}^2}, \quad (80)$$

$$\Gamma_1 = \frac{A_{11}}{\theta_1} - \frac{R_{11}}{i\omega\theta_1}, \quad (81)$$

$$\Gamma_2 = \frac{A_{22}}{\theta_2} - \frac{R_{22}}{i\omega\theta_2}, \quad (82)$$

$$\Lambda_1 = \tilde{\rho}_1 \theta_1 + \frac{R_{11}}{i\omega\theta_1}. \quad (83)$$

In these equations β_{p_1, p_2, p_3}^I and $\beta_{p_1, p_2, p_3}^{II}$ denote the factors connecting the amplitude of the displacement of the two fluid phases to the solid displacement for the three compressional waves P1, P2 and P3. These factors depend on the velocity of each type of compressional wave.

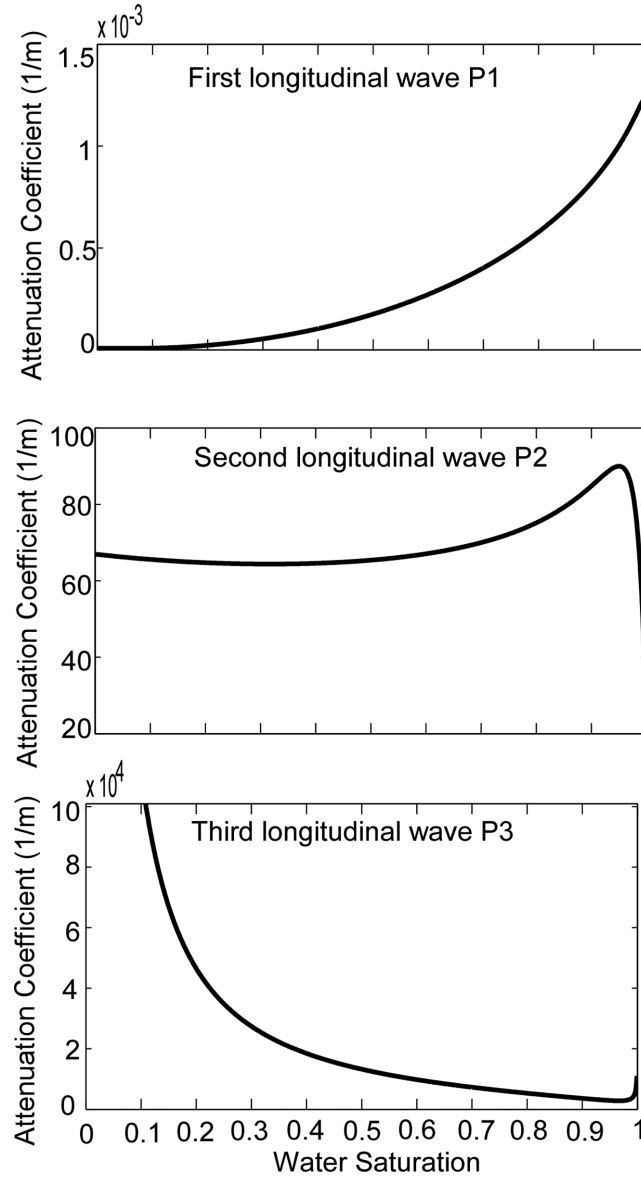


Figure 6. Effect of water saturation on the attenuation of the three P waves calculated from the imaginary components of the roots of cubic eq. (74). The attenuation of the first wave is very small comparing to the strong attenuation of the P2 and P3 waves.

The electric field generated by the propagation of the P1-waves in a homogenous medium drives a conduction current $\mathbf{J}_c = \sigma^*(\omega)\mathbf{E}$ that is exactly counterbalanced by the streaming current \mathbf{J}_s in such a way that the total current density is equal to zero. The conductivity $\sigma^*(\omega)$ denotes the complex conductivity of the porous material at the angular frequency ω . Therefore writing

$$\mathbf{J} = \sigma^*(\omega)\mathbf{E} + \frac{\hat{Q}_2^0}{S_2}\dot{\mathbf{w}}_2 = 0, \quad (84)$$

leads to,

$$\mathbf{E} = j\omega \frac{\hat{Q}_{V2}(\omega)}{\sigma^*(\omega)S_2} \beta_{p_1, p_2, p_3}^{II}(\omega) U \exp[j(kx - \omega t)] \hat{\mathbf{x}}. \quad (85)$$

We reformulate the different parameters in the low-frequency domain as:

$$\hat{Q}_{V2}(\omega) \approx \hat{Q}_{V2}^0, \quad (86)$$

$$\beta_{p_1}^{II}(\omega) \approx \frac{j\omega k_0 k_r \rho_2}{\eta_2}. \quad (87)$$

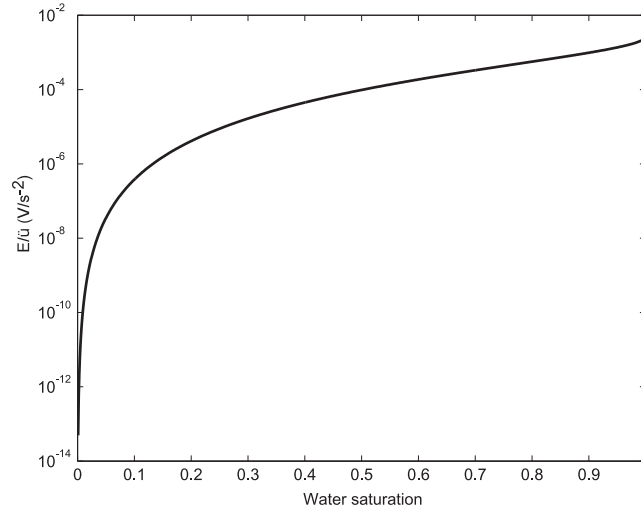


Figure 7. The transfer function linking the seismoelectric field and the grains acceleration plotted as function of water saturation. The transfer function increases with increasing water saturation.

If we also neglect induced polarization effect (in addition to neglecting the electroosmotic effect on the complex electrical conductivity $\sigma^*(\omega)$, see Pride 1994), we have,

$$\sigma^*(\omega) = \sigma_0, \quad (88)$$

where σ_0 denotes the DC conductivity of the material. Therefore, the co-seismic electrical field can be written as:

$$\mathbf{E} = \frac{\hat{Q}_{V2}}{\sigma_0(S_2)S_2} K_r(S_2) \ddot{\mathbf{u}}, \quad (89)$$

where $\ddot{\mathbf{u}}$ denotes the acceleration of the wave and the function K_r is defined by

$$K_r(S_2) = \frac{k_0 k_r(S_2) \rho_2}{\eta_2}. \quad (90)$$

We can also write eq. (89) as,

$$\frac{\mathbf{E}}{\ddot{\mathbf{u}}} \sim C_0 \frac{k_r(S_2)}{S_2} \rho_2, \quad (91)$$

where C_0 denotes the streaming potential coupling coefficient at low frequencies. This coupling coefficient is defined by,

$$C_0 = \frac{\hat{Q}_2^0 k_0 \rho_2 g}{\sigma_0(S_2) \eta_2}, \quad (92)$$

where g denotes the acceleration of the gravity (in $\text{m}^2 \text{s}^{-1}$). Eq. (91) connects the electrical field recorded between two electrodes in the $\hat{\mathbf{x}}$ -direction and the acceleration of the seismic compressional P1 wave. According to eqs (91) and (92), the transfer function depends directly on the saturation S_2 of the wetting phase and on the hydraulic and electrical conductivities, which both depend on the saturation. A simple computation of the transfer function $\mathbf{E}/\ddot{\mathbf{u}}$ shows that it increases with the water content (Fig. 7). Strahser *et al.* (2011) expressed this transfer equation for the normalized seismoelectric field as a power law of the effective saturation by $\mathbf{E}/\ddot{\mathbf{u}} \propto C_0 S_e^{(0.42 \pm 0.25)\alpha} \rho_2$ where C_0 denotes the steady-state streaming potential coupling in the saturated conditions given above. So eq. (91) derived above from the underlying physics of the problem provides a physical basis for the empirical equation obtained by Strahser *et al.* (2011).

3.2. Numerical simulation of the coseismic disturbance

We now use the finite-element method to solve the poroelastic and electric couplings for a homogeneous and partially saturated medium. The field equations described in Section 2 are implemented into Matlab and Comsol 3.5 in order to check the proportionality between the seismic and the electrical signals. The size of the model is $400 \times 400 \text{ m}^2$ with a perfectly matched layer (PML) layer of 50 m surrounding the domain of interest. The material properties required to solve the problems are given in Table 1.

A seismic source is placed at the centre of the domain with a dominant frequency of 10 Hz. The simulation is realized for two values of the water saturation $S_2 = 0.2$ and $S_2 = 0.9$. Fig. 8 shows that the numerical simulations are in agreement with the transfer function corresponding to eq. (89). Both signals are computed for electric and seismic sensors positioned 100 m from the seismic source. The transfer function (between seismic and electric fields) is useful to provide certain hydraulic and electrical parameters. Since the seismoelectric response is due to the existence of the water content in the porous medium, we also studied the amplitude of the co-seismic electric potential with respect to the water saturation in the air–water case.

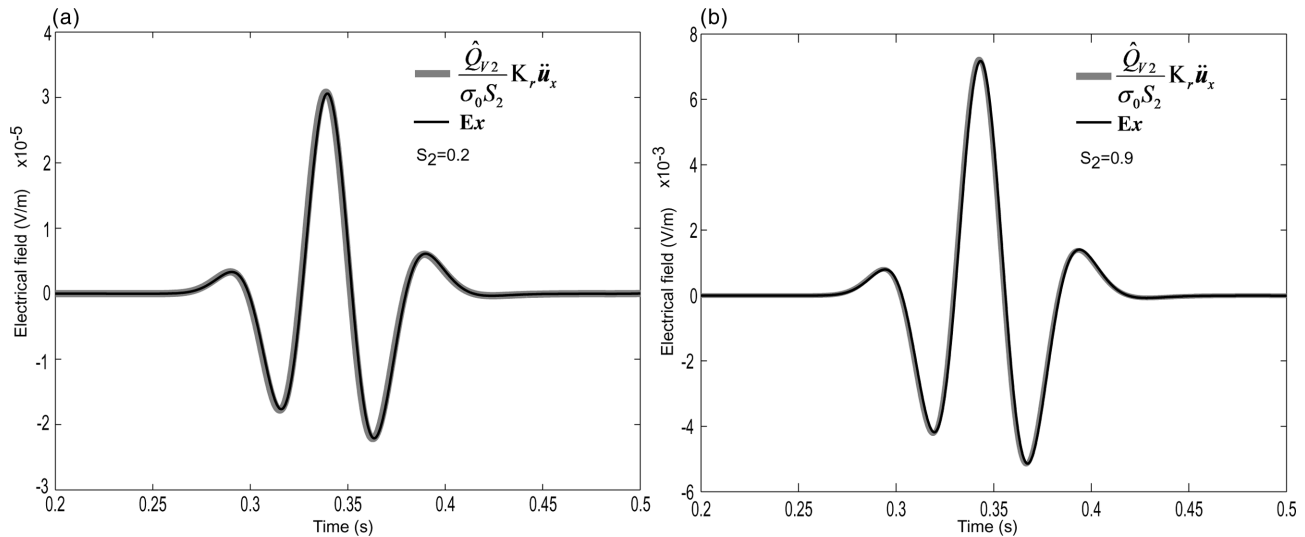


Figure 8. Numerical test to confirm the validity of the transfer function E_x / \ddot{u}_x with two values of the water saturation. The signals are computed 100 m away from the seismic source. The homogenous porous medium is characterized by the properties listed in Table 1.

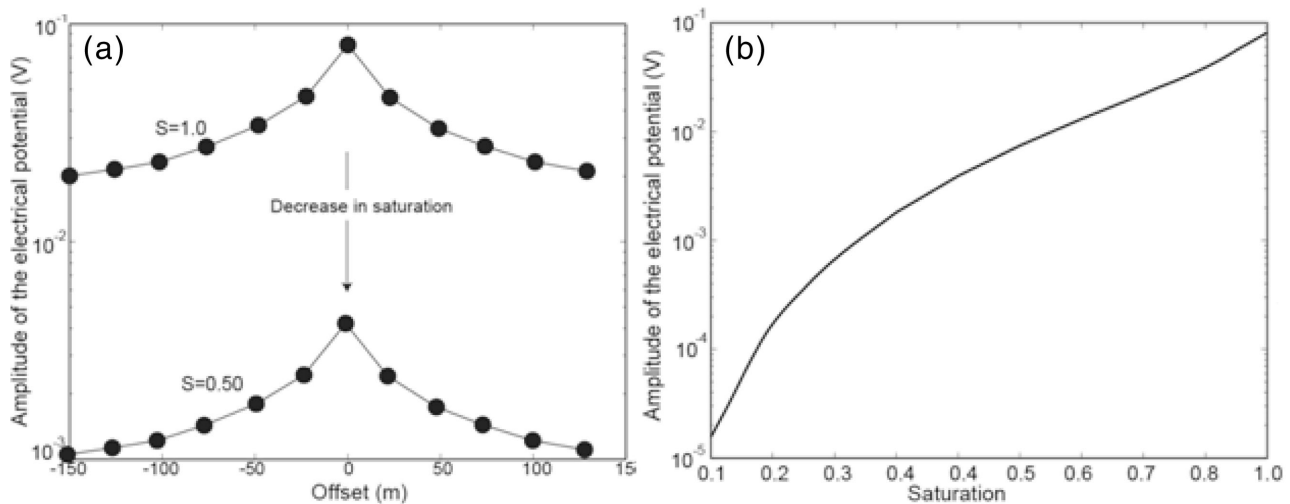


Figure 9. Amplitude of the electrical potential as a function of the saturation. (a) The effect of the water saturation on the coseismic response recorded at the electrodes located at the ground surface. The filled circles correspond to the numerical simulations while the plain broken lines are just here to guide the eyes. (b) Effect of water saturation on the maximum of the amplitude of the coseismic electrical potential response (at offset zero).

We numerically simulated the coseismic signal using different values of the water saturation and we studied the variations of the amplitude of the electrical potential (Fig. 9). The numerical results show an increase in the amplitude of the coseismic electrical disturbance with water saturation. As expected, coseismic electrical signals are vanishingly small at low water saturations and reach a maximum in fully water-saturation conditions (see also Warden *et al.* 2013).

3.3 Seismoelectric conversion

We now look at the ability of the seismoelectric method to remotely detect saturation contrasts using the seismoelectric conversion at a saturation front. We consider two tabular layers in a domain corresponding to $400 \text{ m} \times 400 \text{ m}$. The upper layer has properties that are characteristics of a shallow unsaturated layer and the second, deeper, layer simulates a fully water-saturated aquifer (Fig. 10). The petrophysical parameters of the two layers differ only by the water saturation. Therefore, in absence of a saturation contrast, the domain would be homogeneous. The simulations were realized with three values of the water saturations in the vadose zone, $S_2 = 0.1$, $S_2 = 0.5$ and $S_2 = 0.8$.

The numerical results obtained in Fig. 10 point out that the seismoelectric the interface response can be detected in the simulations when there is a significant saturation contrast between the vadose and saturated zones. Fig. 11 shows that the conversion response is identifiable in the first and the second cases corresponding to $S_2 = 0.1$ and $S_2 = 0.5$ with an increase of the amplitude of the coseismic signature with the increase of the water saturation in the vadose zone. However, in the third case when the saturation of the vadose zone takes the value $S_2 = 0.8$, the amplitude of the interface response is very weak in comparison with the coseismic signal and is difficult to identify

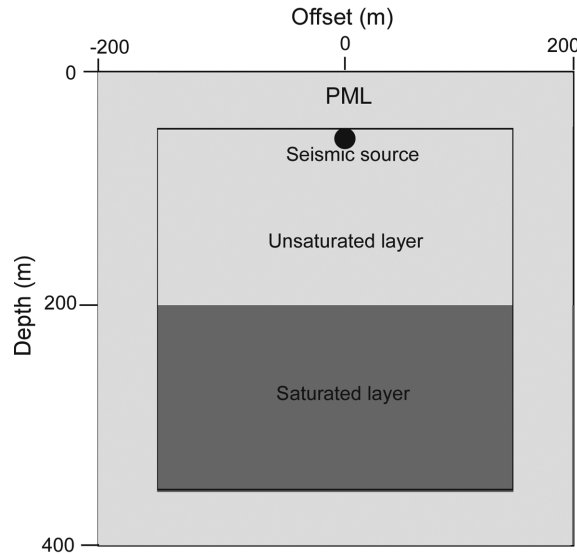


Figure 10. Sketch of the model used for the simulations. The electrodes are collocated at $z = 60$ m. All the electrodes are assumed to be connected to a reference electrode to compute the electrical potential.

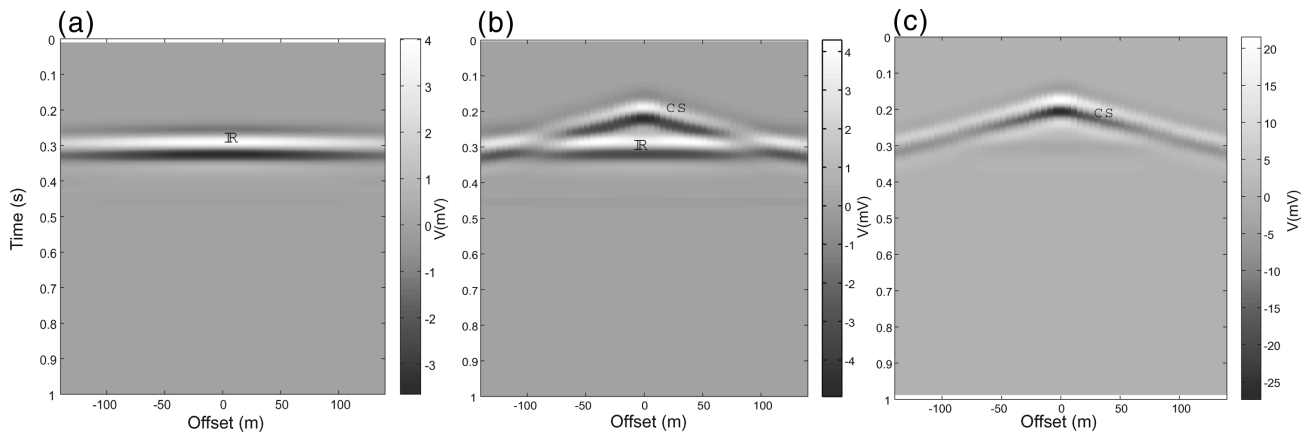


Figure 11. The electric potential generated with our modelling code for three values of the water saturation of the vadose zone $S_2 = 0.1$, $S_2 = 0.5$ and $S_2 = 0.8$. The interface response at 0.28 s can be distinguished when the saturation contrast between the fluid saturated layer and vadose zone is large enough to generate a significant amplitude for the seismoelectric conversion. However, for the last case under study, the contrast is very weak and we observe that it is difficult to detect the interface response.

(Figs 11 and 12). In Fig. 11, we show the simulated electric potential time-series for three values of the water saturations of the vadose zone ($S_2 = 0.1$, $S_2 = 0.5$, and $S_2 = 0.8$). The interface response at 0.28 s can be clearly distinguished in the time-series only when the saturation contrast between the fluid saturated layer and vadose zone is large enough. The seismoelectric interface response can be detected in the simulations when there is a significant saturation contrast between the vadose and saturated zones (see also Warden *et al.* 2013). The same result is shown in Fig. 12 in which we analysed the variations of the amplitude of the interface response due only to the saturation contrast between the saturated and vadose zones.

We conclude therefore from these numerical tests that a dry vadose zone is the best condition to identify the groundwater level because the coseismic signal is expected to be small in comparison to the seismoelectric interface response. This result is consistent with the field observation reported by Strahser *et al.* (2011), who conducted several seismoelectric surveys characterized by different saturation conditions. It would be interesting to use the present theory to simulate the type of field case study presented by Dupuis *et al.* (2007).

A last point to discuss is the advantage of the formulation in term of the speed of the numerical computation. For the present simulation, the computation time was reduced from 351 s using the $(u-w)$ formulation to 116 s using the (u, p) formulation.

4 CONCLUSION

The following conclusions have been obtained:

(1) We have presented a seismoelectric model for heterogeneous deformable porous media saturated with two immiscible Newtonian fluid phases. The influence of the capillary pressure and the inertial effects of the two fluids have been included in the set of the partial differential

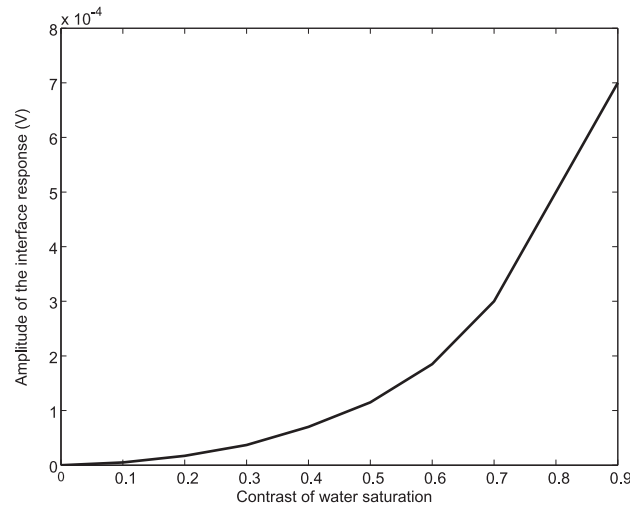


Figure 12. The variations of the amplitude of the interface response due only to the saturation contrast between the saturated and vadose zones. The seismoelectric interface response can be detected in the simulations when there is a significant saturation contrast between the vadose and saturated zones.

equations describing the motion of the hydromechanical disturbances in the form of seismic waves. The analysis of the dispersion relation of the compressional waves derived from these coupled partial differential equations of the poroelastic problem reveals three *P*-wave modes. The first (fast or classical) *P*-wave (*P*1) results from in phase motion of the solid framework and of the two pore fluids with a velocity that can be expressed in the low frequency domain as the square root of the ratio of the effective bulk modulus to an effective density of the medium. The *P*2 and *P*3 slow and waves are diffusive disturbances that are quickly damped. The wave *P*2 is due to out-of-phase motions of the solid framework with respect to the fluids. The wave *P*3 results from the capillary pressure fluctuations. Both *P*2 and *P*3 waves are extremely difficult to observe in the real field conditions. Each of these modes is expected to be associated with a seismoelectric effect of electrokinetic nature, which could be used in turn to identify these wave modes.

(2) Rather than using the displacement of the solid phase and the relative displacements of the two fluid phases as unknown at each node in the formulation of the hydromechanical problem, we use a (u, p) -formulation in which the entire problem is described in terms of the displacement of the solid phase and the fluid pressures of the two fluids. This formulation is new for the two-phase flow problem. It allows us to speed up the numerical computation by reducing the number of unknowns (from 6 to 4 in 2-D).

(3) The electrokinetic formulation used to simulate the seismoelectric signal is based on the recently introduced concept of effective charge density that can be dragged by the flow of the pore water. For each fluid phase, the corresponding effective charge density can be directly related to the permeability of the porous material and relative permeabilities for each fluid phase, therefore avoiding the introduction of parameters that can be difficult to assess independently in field applications.

(4) The partial differential equations have been introduced in a finite element package to numerically simulate the signals seismoelectric in partially saturated media or two-phase flow conditions. We also formulated an analytical transfer function connecting the macroscopic electrical field to the seismic acceleration of the solid phase for the coseismic field. This analytical expression explicitly shows the influence of the water content on the amplitude of the coseismic electrical disturbance. The numerical results showed that the amplitude of this coseismic electrical disturbance is very sensitive to the water content with an increase of its amplitude with water saturation.

(5) We also studied the seismoelectric conversion (interface response) at the interface between a partially saturated layer and a fully saturated layer. We found that the seismoelectric interface response can be identified when the saturation contrasts between the vadose zone and saturated layer is very important (>0.5). Therefore, a dry vadose zone is the best condition to identify the groundwater level because the coseismic signal is small compared to the interface response.

ACKNOWLEDGEMENTS

We thank the Colorado School of Mines Unconventional Natural Gas and Oil Institute (UNGI) CIMMM Consortium sponsors for the support of this research. We thank the editor and the referee for their very useful comments and their time.

REFERENCES

- Ahmad, M.U., 1964. A laboratory study of streaming potentials, *Geophys. Prospect.*, **12**(1), 49–64.
- Alkafef, S., Gochin, R.J. & Smith, A.L., 2001. The effect of double layer overlap on measured streaming currents for toluene flowing through sandstone cores, *Coll. Surf. A: Physiochem. Eng. Aspects*, **195**, 77–80.
- Araji, A., Revil, A., Jardani, A., Minsley, B. & Karaoulis, M., 2012. Imaging with cross-hole seismoelectric tomography, *Geophys. J. Int.*, **188**, 1285–1302.
- Berryman, J.G., Thigpen, L. & Chin, R.C.Y., 1988. Bulk elastic wave propagation in partially saturated porous solids, *J. acoust. Soc. Am.*, **84**(1), 360–373.
- Biot, M.A., 1956a. Theory of propagation of elastic waves in a fluid saturated porous solid, I. Low-frequency range, *J. acoust. Soc. Am.*, **28**(2), 168–178.

- Biot, M.A., 1956b. Theory of propagation of elastic waves in a fluid saturated porous solid, II. Higher frequency range, *J. acoust. Soc. Am.*, **28**(2), 179–191.
- Biot, M.A., 1962. Mechanics of deformation and acoustic propagation in porous media, *J. appl. Phys.*, **33**(4), 1482–1498.
- Bolève, A., Crespy, A., Revil, A., Janod, F. & Mattiuzzo, L., 2007. Streaming potentials of granular media: influence of the Dukhin and Reynolds numbers, *J. geophys. Res.*, **112**, B08204, doi:10.1029/2006JB004673.
- Bordes, C., Jouniaux, L., Garambois, S., Dietrich, M., Pozzi, J.-P. & Gaffet, S., 2008. Evidence of the theoretically predicted seismo-magnetic conversion, *Geophys. J. Int.*, **174**, 489–504.
- Butler, K.E., 1996. Seismoelectric effects of electrokinetic origin, *PhD thesis*, University of British Columbia.
- Casagrande, L., 1983. Stabilization of soils by means of electro-osmosis: state of art, *J. Boston Soc. Civil Eng.*, **69**(2), 255–302.
- Dupuis, J.C., Butler, K.E. & Keping, A.E., 2007. Seismoelectric imaging of the vadose zone of a sand aquifer, *Geophysics*, **72**(6), A81–A85.
- Dupuis, J.C., Butler, K.E., Keping, A.W. & Harris, B.D., 2009. Anatomy of a seismoelectric conversion: measurements and conceptual modelling in boreholes penetrating a sandy aquifer, *J. geophys. Res.*, **114**, B10306, doi:10.1029/2008JB005939.
- Frenkel, J., 1944. On the theory of seismic and seismoelectric phenomena in a moist soil, *J. Phys. J. Phys. (Soviet)*, **8**, 4, 230–241.
- Friberg, J., 1996. Experimental and theoretical investigations into the streaming potential phenomenon with special reference to applications in glaciated terrain, *PhD thesis*, Lulea University of Technology, Sweden.
- Garambois, S. & Dietrich, M., 2001. Seismoelectric wave conversions in porous media: field measurements and transfer function analysis, *Geophysics*, **66**(5), 1417–1430.
- Garambois, S. & Dietrich, M., 2002. Full-waveform numerical simulations of seismo-electromagnetic wave conversions in fluid-saturated stratified porous media, *J. geophys. Res.*, **107**(B7), 2148, doi:10.1029/2001JB000316.
- Haartsen, M.W. & Pride, S.R., 1997. Electrostatic waves from point sources in layered media, *J. geophys. Res.*, **102**(B11), 24 745–24 769.
- Haines, S.S. & Pride, S.R., 2006. Seismoelectric numerical modeling on a grid, *Geophysics*, **71**(6), N57–N65.
- Haines, S.S., Pride, S.R., Klempner, S.L. & Biondi, B., 2007. Seismoelectric imaging of shallow targets, *Geophysics*, **72**(2), G9–G20.
- Ivanov, A.G., 1939. Effect of electrization of earth layers by elastic waves passing through them, in *Proceedings of the USSR Academy of Sciences (Dokl. Akad. Nauk SSSR)*, Vol. 24, pp. 42–45.
- Jardani, A., Revil, A., Bolève, A., Dupont, J.P., Barrash, W. & Malama, B., 2007. Tomography of the Darcy velocity from self-potential measurements, *Geophys. Res. Lett.*, **34**, L24403, doi:10.1029/2007GL031907.
- Jardani, A., Revil, A., Slob, E. & Söllner, W., 2009. Stochastic joint inversion of 2D seismic and seismoelectric signals in linear poroelastic materials: a numerical investigation, *Geophysics*, **75**(1), N19–N31.
- Jougnot, D. & Linde, N., 2013. Self-potentials in partially saturated media: the importance of explicit modeling of electrode effects, *Vadose Zone J.*, **12**(2), doi:10.2136/vzj2012.0169.
- Jougnot, D., Linde, N., Revil, A. & Doussan, C., 2012. Derivation of soil-specific streaming potential electrical parameters from hydrodynamic characteristics of partially saturated soils, *Vadose Zone J.*, **11**(1), doi:10.2136/vzj2011.0086.
- Kulesa, B., Murray, T. & Rippin, D., 2006. Active seismoelectric exploration of glaciers, *Geophys. Res. Lett.*, **33**, L07503, doi:10.1029/2006GL025758.
- Leroy, P., Jougnot, D., Revil, A., Lassin, A. & Azaroual, M., 2012. A double layer model of the gas bubble/water interface, *J. Colloid Interf. Sci.*, **388**(1), 243–256.
- Linde, N., Jougnot, D., Revil, A., Matthäi, S.K., Arora, T., Renard, D. & Doussan, C., 2007. Streaming current generation in two-phase flow conditions, *Geophys. Res. Lett.*, **34**(3), L03306, doi:10.1029/2006GL028878.
- Lo, W.C., Sposito, G. & Mayer, E., 2002. Immiscible two-phase fluid flows in deformable porous media, *Adv. Water Resour.*, **25**, 1105–1117.
- Lo, W.C., Sposito, G. & Majer, E., 2005. Wave propagation through elastic porous media containing two immiscible fluids, *Water Resour. Res.*, **41**, W02025, doi:10.1029/2004WR003162.
- Mahardika, H., Revil, A. & Jardani, A., 2012. Waveform joint inversion of seismograms and electrograms for moment tensor characterization of fracking events, *Geophysics*, **77**(5), ID23–ID39.
- Martner, S.T. & Sparks, N.R., 1959. The electrostatic effect, *Geophysics*, **24**(2), 297–308.
- Neev, J. & Yeatts, F.R., 1989. Electrokinetic effects in fluid-saturated poroelastic media, *Phys. Rev. B*, **40**(13), 9135–9141.
- Pain, C.C., Saunders, J.H., Worthington, M.H., Singer, J.M., Stuart-Bruges, W., Mason, G. & Goddard, A., 2005. A mixed finite-element method for solving the poroelastic Biot equations with electrokinetic coupling, *Geophys. J. Int.*, **160**, 592–608.
- Parkhomenko, E. & Gaskarov, I., 1971. Borehole and laboratory studies of the seismoelectric effect of the second kind in rocks, *Izv. Akad. Sci. USSR, Phys. Solid Earth*, **9**, 663–666.
- Pengra, D.S., Li, S.X. & Wong, P., 1999. Determination of rock properties by low-frequency AC electrokinetics, *J. geophys. Res.*, **104**, 485–508.
- Pride, S., 1994. Governing equations for the coupled electromagnetics and acoustics of porous media, *Phys. Rev. B*, **50**, 15 678–15 696.
- Pride, S.R. & Garambois, S., 2005. Electrostatic wave theory of Frenkel and more recent developments, *J. Eng. Mech.*, **131**(9), 898–907.
- Pride, S.R. & Haartsen, M.W., 1996. Electrostatic wave properties, *J. acoust. Soc. Am.*, **100**, 1301–1315.
- Revil, A., 2012. Spectral induced polarization of shaly sands: Influence of the electrical double layer, *Water Resour. Res.*, **48**, W02517, doi:10.1029/2011WR011260.
- Revil, A., 2013a. Effective conductivity and permittivity of unsaturated porous materials in the frequency range 1 mHz–1GHz, *Water Resour. Res.*, **49**, 306–327.
- Revil, A., 2013b. On charge accumulations in heterogeneous porous materials under the influence of an electrical field, *Geophysics*, **78**(4), D271–D291.
- Revil, A. & Jardani, A., 2010. Seismoelectric response of heavy oil reservoirs. Theory and numerical modelling, *Geophys. J. Int.*, **180**, 781–797.
- Revil, A. & Leroy, P., 2001. Hydroelectric coupling in a clayey material, *Geophys. Res. Lett.*, **28**(8), 1643–1646.
- Revil, A. & Mahardika, H., 2013. Coupled hydromechanical and electromagnetic disturbances in unsaturated porous materials, *Water Resour. Res.*, **49**, doi:10.1002/wrcr.20092.
- Revil, A., Schwaeger, H., Cathles, L.M. III & Manhardt, P.D., 1999. Streaming potential in porous media: 2. Theory and application to geothermal systems, *J. geophys. Res.*, **104**(B9), 20 033–20 048.
- Revil, A., Leroy, P. & Titov, K., 2005. Characterization of transport properties of argillaceous sediments. Application to the Callovo-Oxfordian Argillite, *J. geophys. Res.*, **110**, B06202, doi:10.1029/2004JB003442.
- Revil, A., Linde, N., Cerepi, A., Jougnot, D., Matthäi, S. & Finsterle, S., 2007. Electrokinetic coupling in unsaturated porous media, *J. Colloid Interface Sci.*, **313**(1), 315–327.
- Revil, A., Barnier, G., Karaoulis, M. & Sava, P., 2014. Seismoelectric coupling in unsaturated porous media: theory, petrophysics, and saturation front localization using an electroacoustic approach, *Geophys. J. Int.*, **196**(2), 867–884.
- Santos, J.E., 2011. Finite element approximation of coupled seismic and electromagnetic waves in fluid-saturated poroviscoelastic media, *Numer. Methods Partial Differ. Equat.*, **27**(2), 351–386.
- Santos, J.E., Corbero, J.M. & Douglas, J., 1990a. Static and dynamic behavior of a porous solid saturated by a two-phase fluid, *J. acoust. Soc. Am.*, **87**(4), 1428–1438.
- Santos, J.E., Douglas, J., Corbero, J. & Lovera, O.M., 1990b. A model for wave propagation in a porous medium saturated by a two-phase fluid, *J. acoust. Soc. Am.*, **87**(4), 1439–1448.
- Santos, J.E., Ravazzoli, C.L., Gauzelloni, P.M., Carcione, J.M. & Cavallini, F., 2004. Simulation of waves in poro-viscoelastic rocks saturated by immiscible fluids. Numerical evidence of a second slow wave, *J. Comput. Acoust.*, **12**(1), 1–21.

- Sheffer, M.R., 2007. Forward modeling and inversion of streaming potential for the interpretation of hydraulic conditions from self-potential data, *PhD thesis*, University of British Columbia.
- Strahser, M., Jouniaux, L., Sailhac, P., Matthey, P. & Zillmer, M., 2011. Dependence of seismoelectric amplitudes on water content, *Geophys. J. Int.*, **187**(3), 1378–1392.
- Tarback, T.L., Ota, S.T. & Richmond, G.L., 2006. Spectroscopic studies of solvated hydrogen and hydroxide ions at aqueous surfaces, *J. Am. Chem. Soc.*, **128**, 14 519–14 527.
- Tuncay, K. & Corapcioglu, M.Y., 1996. Body waves in poroelastic media saturated by two immiscible fluids, *J. geophys. Res.*, **111**(B11), 25 149–25 159.
- Tuncay, K. & Corapcioglu, M.Y., 1997. Wave propagation in poroelastic media saturated by two fluids, *J. Appl. Mech.*, **64**(2), 313–320.
- Van Genuchten, M.T., 1980. A closed-form equation for predicting the hydraulic conductivity of unsaturated soils, *Soil Sci. Soc. Am. J.*, **44**(5), 892–898.
- Vasco, D.W. & Minkoff, S.E., 2012. On the propagation of a disturbance in a heterogeneous, deformable, porous medium saturated with two fluid phases, *Geophysics*, **77**(3), L25–L44.
- Warden, S., Garambois, S., Jouniaux, L., Brito, D., Sailhac, P. & Bordes, C., 2013. Seismoelectric wave propagation numerical modelling in partially saturated materials, *Geophys. J. Int.*, **194**(3), 1498–1513.
- Waxman, M.H. & Smits, L.J.M., 1968. Electrical conductivities in oil bearing shaly sands, *Soc. Pet. Eng. J.*, **243**, 107–122.
- Whitman, W.W. & Towle, G.H., 1992. The influence of elastic and density properties on the behavior of the Gassmann relation, *Log Analyst*, **33**, 500–506.
- Zhu, Z. & Toksöz, N., 2012. Experimental measurements of streaming potential and seismoelectric conversion in Berea sandstone, *Geophys. Prospect.*, **78**(3), D143–D150.
- Zyserman, F.I., Gauzellino, P.M. & Santos, J.E., 2010. Finite element modeling of SHTE and PSVTM electroseisms, *J. appl. Geophys.*, **72**(2), 79–91.

APPENDIX A: SOURCE CURRENT DENSITY

We use a volume averaging approach here to determine the total source current density of electrokinetic nature associated with the excess of charge in the non-wetting (1) and wetting (2) fluid phases. We first define the effective (moveable) charge density in quasi-static flow conditions. We write the effective macroscopic charge densities (in $C m^{-3}$) dragged by the flow of the two fluid phases as $\hat{Q}_1^0(S_1)$ and $\hat{Q}_2^0(S_2)$ for the non-wetting and wetting fluid phases, respectively. These charge densities are defined by,

$$\hat{Q}_1^0(S_1) = \frac{\langle \rho_1(\mathbf{x})(\dot{\mathbf{u}}_1(\mathbf{x}) - \dot{\mathbf{u}}(\mathbf{x})) \rangle}{\langle \dot{\mathbf{u}}_1(\mathbf{x}) - \dot{\mathbf{u}}(\mathbf{x}) \rangle}, \quad (A1)$$

$$\hat{Q}_2^0(S_2) = \frac{\langle \rho_2(\mathbf{x})(\dot{\mathbf{u}}_2(\mathbf{x}) - \dot{\mathbf{u}}(\mathbf{x})) \rangle}{\langle \dot{\mathbf{u}}_2(\mathbf{x}) - \dot{\mathbf{u}}(\mathbf{x}) \rangle}, \quad (A2)$$

where the volume averaging operator is defined by

$$\langle . \rangle = \frac{1}{V_p} \int_{V_p} (.) d\tau, \quad (A3)$$

where the brackets denote a pore volume averaging, $\rho_1(\mathbf{x})$ and $\rho_2(\mathbf{x})$ (both in $C m^{-3}$) denotes the local charge density in phases 1 and 2, respectively, $\dot{\mathbf{u}}_1(\mathbf{x}) - \dot{\mathbf{u}}(\mathbf{x})$ and $\dot{\mathbf{u}}_2(\mathbf{x}) - \dot{\mathbf{u}}(\mathbf{x})$ denote the local instantaneous velocity of fluids 1 and 2 with respect to the solid phase (in $m s^{-1}$), \mathbf{x} a local position in the pore space of the material (in fluid phases 1 and 2, and $d\tau$ an elementary volume around point $M(\mathbf{x})$, and $\dot{\mathbf{u}}(\mathbf{x})$ denote the instantaneous local velocity of the solid phase. Eqs (A1) and (A2) are valid whatever the size of the diffuse layer with respect to the size of the pores. These equations are showing that the charge densities $\hat{Q}_1^0(S_1)$ and $\hat{Q}_2^0(S_2)$ are not a static charge densities since their definitions involve the average of the pore water velocity with respect to the solid phase. The macroscopic source current density \mathbf{J}_S (called the streaming current density and expressed in $A m^{-2}$) is related to the local current densities $\mathbf{j}_{1,2}$ defined in the two fluid phase and defined with respect to the deformation of the solid phase by,

$$\mathbf{J}_S = \theta_1 \langle \mathbf{j}_1 \rangle + \theta_2 \langle \mathbf{j}_2 \rangle, \quad (A4)$$

$$\mathbf{J}_S = \theta_1 \langle \rho_1(\dot{\mathbf{u}}_1 - \dot{\mathbf{u}}) \rangle + \theta_2 \langle \rho_2(\dot{\mathbf{u}}_2 - \dot{\mathbf{u}}) \rangle, \quad (A5)$$

$$\mathbf{J}_S = \hat{Q}_1^0(S_1)\theta_1 \langle \dot{\mathbf{u}}_1 - \dot{\mathbf{u}} \rangle + \hat{Q}_2^0(S_2)\theta_2 \langle \dot{\mathbf{u}}_2 - \dot{\mathbf{u}} \rangle, \quad (A6)$$

The filtration displacements are defined by $\mathbf{w}_i = \theta_i \langle \mathbf{u}_i - \mathbf{u} \rangle$ (see eq. 7 of the main text where \mathbf{u}_i and \mathbf{u} denotes local quantities in this appendix while they represent macroscopic, already volume-averaged, quantities in the main text). Therefore the total current density of electrokinetic nature is given by,

$$\mathbf{J}_S = \hat{Q}_1^0(S_1)\dot{\mathbf{w}}_1 + \hat{Q}_2^0(S_2)\dot{\mathbf{w}}_2. \quad (A7)$$

where $\mathbf{w}_i = \tilde{k}_i(\nabla p_i - \omega^2 \rho_i \mathbf{u})$. The last step is to define the effect of the saturation upon the charge densities themselves. We follow here the approach from Revil *et al.* (2007) and we use the following dependencies:

$$\hat{Q}_i^0(S_i) = \frac{\hat{Q}_i^0}{S_i}, \quad (A8)$$

where \hat{Q}_i^0 ($i = 1, 2$) denote the value of the effective charge density at saturation. Note however that other formulations are possible. There are currently a lot of discussions in the literature regarding the saturation dependence of the effective charge densities. Usually the effective charge density of the non-wetting phase is expected to be very small and therefore

$$\mathbf{J}_S \approx \frac{\hat{Q}_2^0}{S_2} \dot{\mathbf{w}}_2, \quad (\text{A9})$$

where \hat{Q}_2^0 can be in turn related to the permeability at saturation as shown in Fig. 4. The expression of the source current density (constitutive equation) can be combined with the conservation of charge $[\nabla \cdot (\sigma \mathbf{E} + \mathbf{J}_S) = 0]$ to obtain eq. (61) of the main text.

APPENDIX B: LONGITUDINAL WAVE MODES

We detail below the expressions of the coefficients used to compute the velocities of the three waves in the longitudinal mode. We start with the complete set of governing equations describing the poroelastic problem in two phase flow conditions:

$$\left\{ -\omega^2 \begin{bmatrix} \rho_s \theta_s & \frac{A_{11}}{\theta_1} & \frac{A_{22}}{\theta_2} \\ \rho_1 \theta_1 & \tilde{\rho}_1 \theta_1 & 0 \\ \rho_2 \theta_2 & 0 & \tilde{\rho}_2 \theta_2 \end{bmatrix} + j\omega \begin{bmatrix} 0 & -\frac{R_{11}}{\theta_1} & -\frac{R_{22}}{\theta_2} \\ 0 & \frac{R_{11}}{\theta_1} & 0 \\ 0 & 0 & \frac{R_{22}}{\theta_1} \end{bmatrix} + k^2 \begin{bmatrix} \tilde{a}_{11} & \frac{a_{12}}{\theta_1} & \frac{a_{13}}{\theta_2} \\ a_{2s} & \frac{a_{22}}{\theta_1} & \frac{a_{23}}{\theta_2} \\ a_{3s} & \frac{a_{23}}{\theta_1} & \frac{a_{33}}{\theta_2} \end{bmatrix} \right\} \begin{bmatrix} U \\ W_1 \\ W_2 \end{bmatrix} = \begin{bmatrix} 0 \\ 0 \\ 0 \end{bmatrix}. \quad (\text{B1})$$

The equation can be also written as

$$\begin{bmatrix} \pi_s - \tilde{a}_{11} \tau & \chi_1 - \frac{a_{12}}{\theta_1} \tau & \chi_2 - \frac{a_{13}}{\theta_2} \tau \\ \pi_1 - a_{2s} \tau & \gamma_1 - \frac{a_{22}}{\theta_1} \tau & -\frac{a_{23}}{\theta_2} \tau \\ \pi_2 - a_{3s} \tau & -\frac{a_{22}}{\theta_1} \tau & \gamma_2 - \frac{a_{33}}{\theta_2} \tau \end{bmatrix} \begin{bmatrix} U \\ W_1 \\ W_2 \end{bmatrix} = \begin{bmatrix} 0 \\ 0 \\ 0 \end{bmatrix}, \quad (\text{B2})$$

where

$$\tau = k^2, \quad (\text{B3})$$

$$\pi_s = \omega^2 \rho_s \theta_s, \quad (\text{B4})$$

$$\pi_1 = \omega^2 \rho_1 \theta_1, \quad (\text{B5})$$

$$\pi_2 = \omega^2 \rho_2 \theta_2, \quad (\text{B6})$$

$$\chi_1 = \omega^2 \frac{A_{11}}{\theta_1} - j\omega \frac{R_{11}}{\theta_1}, \quad (\text{B7})$$

$$\chi_2 = \omega^2 \frac{A_{22}}{\theta_2} - j\omega \frac{R_{22}}{\theta_2}, \quad (\text{B8})$$

$$\gamma_1 = \omega^2 \tilde{\rho}_1 \theta_1 + j\omega \frac{R_{11}}{\theta_1}, \quad (\text{B9})$$

$$\gamma_2 = \omega^2 \tilde{\rho}_2 \theta_2 + j\omega \frac{R_{22}}{\theta_1}. \quad (\text{B10})$$

The existence of a solution to eq. (B2) requires that the determinant of the matrix must vanish.

$$\det \begin{bmatrix} \pi_s - \tilde{a}_{11} \tau & \chi_1 - \frac{a_{12}}{\theta_1} \tau & \chi_2 - \frac{a_{13}}{\theta_2} \tau \\ \pi_1 - a_{2s} \tau & \gamma_1 - \frac{a_{22}}{\theta_1} \tau & -\frac{a_{23}}{\theta_2} \tau \\ \pi_2 - a_{3s} \tau & -\frac{a_{22}}{\theta_1} \tau & \gamma_2 - \frac{a_{33}}{\theta_2} \tau \end{bmatrix} = 0. \quad (\text{B11})$$

The determinant can be expressed as (see Vasco & Minkoff 2012):

$$Q_3 \tau^3 + Q_2 \tau^2 + Q_1 \tau + Q_0 = 0, \quad (\text{B12})$$

with

$$Q_3 = \det \begin{bmatrix} \tilde{a}_{11} & a_{12} & a_{13} \\ a_{2s} & a_{22} & a_{23} \\ a_{3s} & a_{23} & a_{33} \end{bmatrix}, \quad (\text{B13})$$

$$Q_2 = \det \begin{bmatrix} \pi_s & a_{12} & a_{13} \\ \pi_1 & a_{22} & a_{23} \\ \pi_2 & a_{23} & a_{33} \end{bmatrix} + \det \begin{bmatrix} \tilde{a}_{11} & \chi_1 & a_{13} \\ a_{2s} & \gamma_1 & a_{23} \\ a_{3s} & 0 & a_{33} \end{bmatrix} + \det \begin{bmatrix} \tilde{a}_{11} & a_{12} & \chi_2 \\ a_{2s} & a_{22} & 0 \\ a_{3s} & a_{23} & \gamma_2 \end{bmatrix}, \quad (\text{B14})$$

$$Q_1 = \det \begin{bmatrix} \pi_s & \chi_1 & a_{13} \\ \pi_1 & \gamma_1 & a_{23} \\ \pi_2 & 0 & a_{33} \end{bmatrix} + \det \begin{bmatrix} \pi_s & a_{12} & \chi_2 \\ \pi_1 & a_{23} & 0 \\ \pi_2 & a_{33} & \gamma_2 \end{bmatrix} + \det \begin{bmatrix} \tilde{a}_{11} & \chi_1 & \chi_2 \\ a_{2s} & \gamma_1 & 0 \\ a_{2s} & 0 & \gamma_2 \end{bmatrix}, \quad (\text{B15})$$

$$Q_0 = \det \begin{bmatrix} \tilde{a}_{11} & \chi_1 & \chi_2 \\ \pi_1 & \gamma_1 & 0 \\ \pi_2 & 0 & \gamma_2 \end{bmatrix}. \quad (\text{B16})$$

The solution of the cubic eq. (B12) is determined using a code written in Matlab.